ACS Chemical Neuroscience
Cite This: ACS Chem. Neurosci. XXXX, XXX, XXX−XXX
Research Article
pubs.acs.org/chemneuro

Fluorescent 1,4-Naphthoquinones To Visualize Diffuse and Dense-Core Amyloid Plaques in APP/PS1 Transgenic Mouse Brains

Naewoo Neo Shin,[†] Hanna Jeon,[‡] Youngeun Jung,[‡] Seungyeop Baek,[‡,∥] Sejin Lee,[‡] Hee Chan Yoo,[‡] Gi Hun Bae,[‡] Keunwan Park,[⊥] Seung-Hoon Yang,[§] Jung Min Han,[‡] Ikyon Kim,*[,‡] and YoungSoo Kim*[,†,‡]

[†]Integrated Science and Engineering Division, Yonsei University, Incheon 21983, Republic of Korea
[‡]Department of Pharmacy and Yonsei Institute of Pharmaceutical Science, Yonsei University, Incheon 21983, Republic of Korea
[∥]Department of Biotechnology, Yonsei University, Seoul 03722, Republic of Korea
[⊥]Natural Product Informatics Research Center, Korea Institute of Science and Technology, Gangneung 25451, Republic of Korea
[§]Department of Medical Biotechnology, College of Life Science and Biotechnology, Dongguk University, Seoul 04620, Republic of Korea

Supporting Information

ABSTRACT: Recent clinical approvals of brain imaging radiotracers targeting amyloid-β provided clinicians the tools to detect and confirm Alzheimer's disease pathology without autopsy or biopsy. While current imaging agents are effective in postsymptomatic Alzheimer's patients, there is much room for improvement in earlier diagnosis, hence prompting a need for new and improved amyloid imaging agents. Here we synthesized 41 novel 1,4-naphthoquinone derivatives and initially discovered 14 antiamyloidogenic compounds via in vitro amyloid-β aggregation assay; however, qualitative analyses of these compounds produced conflicting results and required further investigation. Follow-up docking and biophysical studies revealed that four of these compounds penetrate the blood-brain barrier, directly bind to amyloid-β aggregates, and enhance fluorescence properties upon interaction. These compounds specifically stain both diffuse and dense-core amyloid-β plaques in brain sections of APP/PS1 double transgenic Alzheimer's mouse models. Our findings suggest 1,4-naphthoquinones as a new scaffold for amyloid-β imaging agents for early stage Alzheimer's.

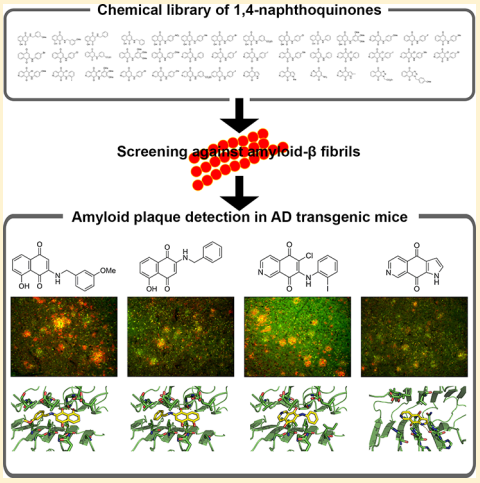

KEYWORDS: *Alzheimer's disease, amyloid, diffuse plaques, 1,4-naphthoquinone, imaging agent, Aβ*

INTRODUCTION

Alzheimer's disease (AD) is the most common neurodegenerative disorder accompanied by extracellular deposition of amyloid-β (Aβ) plaques in the brain.[1] Aβ monomers begin to aggregate into fibrils and eventually plaques in AD patients least a decade before symptomatic onset. Thus, Aβ aggregation has become one of the main targets of AD diagnostic and therapeutic development.[2] Previous reports suggest that the buildup of diffuse Aβ plaques, amorphous deposits that lack dense cores or dystrophic neurites, in the cortex is considered the first pathological change in presymptomatic AD. Although the precise mechanism is still unclear, it is widely believed that diffuse plaques are precursors of dense-core plaques, or amyloid deposits with a compact core surrounded by dystrophic neurites.[3] Current clinically approved amyloid imaging radiotracers are utilized to primarily detect dense-core plaques in patients with mild cognitive impairment and AD; however, this approach encounters limitations when used for presymptomatic diagnosis, as diffuse plaques are more abundant than dense-core plaques during the early stages and produce false positives due to the imaging agents having low affinity toward diffuse plaques.[3] To enhance accuracy for early diagnosis of AD patients, it would be ideal to develop an amyloid imaging agent that specifically labels diffuse plaques in addition to dense-core plaques.

Naphthoquinones (NQ) are colored chemical compounds that exist in nature as secondary metabolites, or organic products that are not directly involved in growth or development.[4,5] Generally, secondary metabolites play a vital role in environmental adaptation, defense mechanisms, photoprotection, and structure stabilization.[6] First discovered as a major component of plants used in many traditional medicines in Asian countries, NQs have garnered considerable interests from researchers due to their antibacterial, antifungal,

Received: February 11, 2019
Accepted: April 15, 2019

DOI: 10.1021/acschemneuro.9b00093
ACS Chem. Neurosci. XXXX, XXX, XXX−XXX

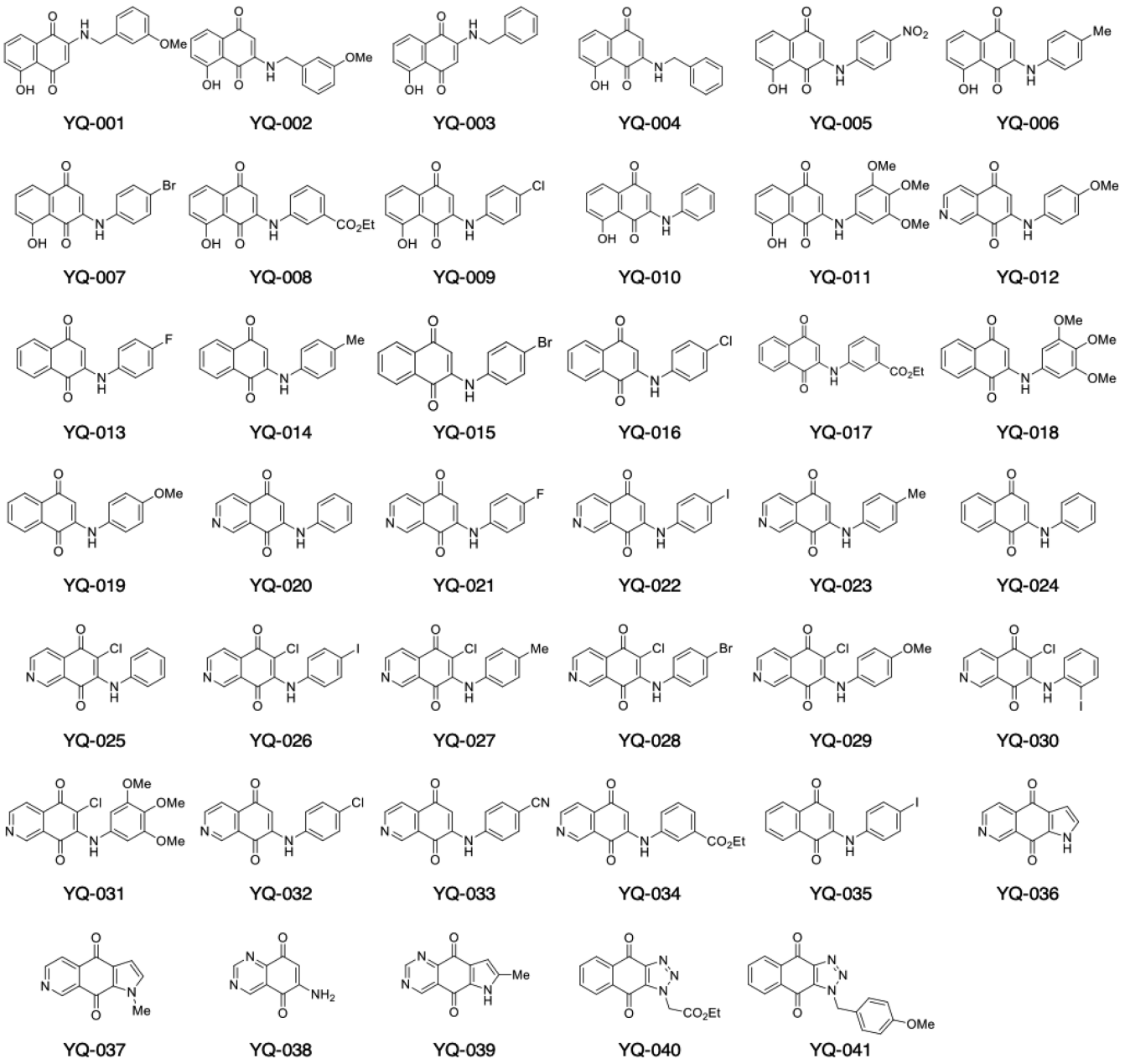

Figure 1. Chemical structures of novel 41 derivatives of 1,4-NQ. A chemical library of 41 novel fluorescent 1,4-naphthoquinone derivatives was synthesized. See also Figure S4 for NMR spectrum data.

antitumor, and insecticidal properties.[7−10] The diverse set of pharmacological activities displayed by this small molecule makes it very attractive as a building block for synthesis of novel drugs. Recent studies also discovered that several derivatives of its most stable isomeric form, 1,4-naphthoquinones (1,4-NQ) can exhibit neuroprotective effects and disrupt Aβ aggregation.[11−15] This suggests that 1,4-NQ derivatives may play a key role in AD treatment.

The original aim of this study was to synthesize and screen novel 1,4-NQ derivatives against Aβ aggregation to identify possible drug candidates for AD. First, we synthesized 41 novel compounds and evaluated the effects of them on Aβ aggregates by conducting Thioflavin T (ThT) fluorescence assay for inhibition of Aβ fibrilization; we then selected 14 compounds to check for dissociation of preformed Aβ aggregates. We discovered discrepancies in our data after performing gel electrophoresis for qualitative analysis, as it was not consistent with our primary results. We suspected that these compounds might interfere with ThT, which binds to β-sheet structures of Aβ plaques, in these studies; as such, we measured the fluorescence spectrum of the selected compounds and found that four emit fluorescence in the presence of Aβ. We also performed histological staining in aged B6C3Tg (APPswe, PSEN 1dE9)85Dbo/J (APP/PS1) double transgenic AD mouse model brains using these compounds and found that they specifically stain Aβ plaques. We further assessed their potential as possible amyloid imaging agents by screening the compounds through an artificial blood-brain barrier (BBB) membrane by parallel artificial membrane permeability assay (PAMPA). Surface plasmon resonance analysis and docking model studies further confirms the strong Aβ-binding affinity of an imaging agent candidate.

DOI: 10.1021/acschemneuro.9b00093
ACS Chem. Neurosci. XXXX, XXX, XXX−XXX

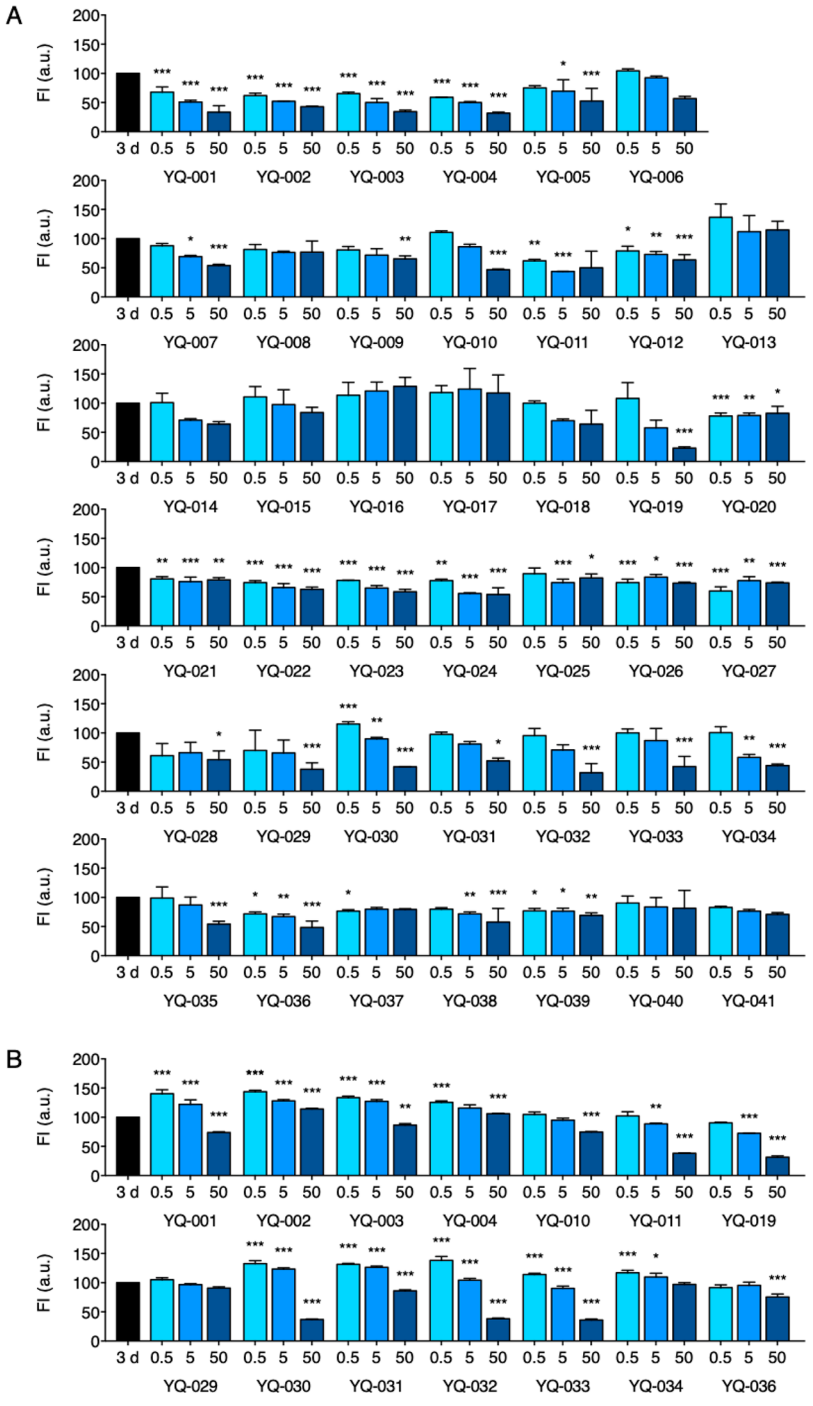

Figure 2. ThT assay for anti-Aβ aggregation activity of 1,4-NQ derivatives. ThT fluorescence assay was conducted for (A) inhibition of Aβ42 aggregation and (B) disaggregation of Aβ42 aggregates using 50 μM Aβ42 with 0.5, 5, or 50 μM YQ compounds as shown. Fluorescence intensities (FI) of all samples were normalized to Aβ aggregates that were incubated for 3 days, or 3 d (100%). Data represents the mean of three repeated experiments $\pm$ SDs, and one-way ANOVA was performed followed by Bonferroni's posthoc comparisons test (*P < 0.033, **P < 0.002, ***P < 0.001).

RESULTS

ThT Assay for Anti-Aβ Aggregation Activity of 1,4-NQ Derivatives. Here we examined whether the synthesized 41 derivatives of 1,4-NQ can inhibit Aβ42 aggregates formation and dissociate preformed Aβ aggregates by conducting ThT fluorescence assay (Figure 1). ThT is a dye that undergoes conformation and fluoresces after binding to cross-β-sheet-rich structures of Aβ aggregates.[16] In inhibition assays, each compound was added to monomeric Aβ42 prior to incubation to induce inhibition. We selected 14 compounds, **YQ-001**, **YQ-002**, **YQ-003**, **YQ-004**, **YQ-010**, **YQ-011**, **YQ-019**, **YQ-029**, **YQ-030**, **YQ-031**, **YQ-032**, **YQ-033**, **YQ-034**, and **YQ-036**, with the highest inhibitory effects on Aβ aggregates (below 50% fluorescence intensity) for the next disaggregation assay to see if they can dissociate pre-existing Aβ42 aggregates (Figure 2A). For the disaggregation assay, Aβ42 aggregates were prepared before mixing with the 1,4-NQ compounds. Among the 14 compounds, we found that 10 compounds, **YQ-**

DOI: 10.1021/acschemneuro.9b00093
ACS Chem. Neurosci. XXXX, XXX, XXX−XXX

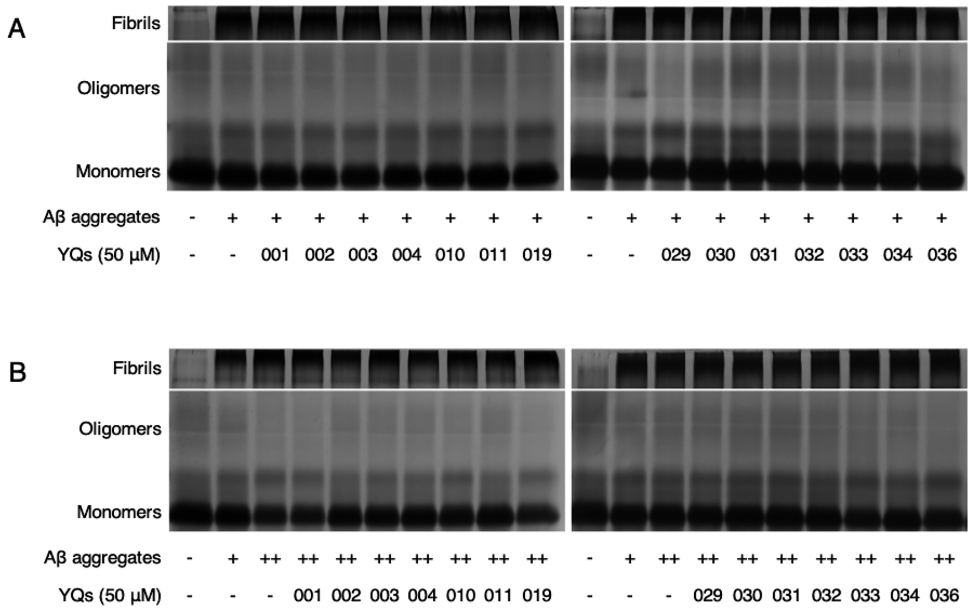

Figure 3. SDS-PAGE analysis to confirm inhibition and disaggregation effects of 1,4-NQ derivatives on Aβ42. Candidate compounds were selected for SDS-PAGE analysis on (A) inhibition of Aβ42 aggregation and (B) disaggregation of Aβ42 aggregates. Samples were incubated for 3 days (+) or 6 days (++) total. Aβ42 samples were prepared by carrying out PICUP chemistry to stabilize oligomer populations and analyzed on 15% gradient polyacrylamide gels. Samples are distributed by monomers (5 kDa), dimers (10 kDa), oligomers (15 to 75 kDa), and larger aggregates or fibrils (trapped at the top of the gels). The products were observed by using silver staining. See also Figure S1.

001, **YQ-003**, **YQ-010**, **YQ-011**, **YQ-019**, **YQ-030**, **YQ-031**, **YQ-032**, **YQ-033**, and **YQ-036**, reduced β-sheet-rich Aβ42 aggregates significantly at 50 μM (Figure 2B). Taken together, ThT fluorescence assay reveals 14 compounds that inhibit aggregation of Aβ and 10 compounds that disaggregate Aβ aggregates.

Gel Electrophoresis To Confirm Anti-Aβ Aggregation Effects of 1,4-NQ Derivatives on Aβ42. Even though ThT is a fluorescent dye regularly used to quantify Aβ fibrils, this colorimetric assay cannot monitor changes in oligomerization. Furthermore, the assay could produce false-positive data as the reduction due to its heavily reliance on ThT binding to β-sheet-rich structures, as reduced fluorescence intensity may be attributed to interference by the 1,4-NQ compounds.[17] Abnormal behaviors of most of chemicals in disaggregation assays support such a possibility by showing levels of fibrils increased in lower dosage (0.5 μM) but reduced in higher dosage (50 μM) (Figure 2B). As such, we performed SDS-PAGE analysis with photoinduced cross-linking of unmodified proteins (PICUP) to visualize Aβ monomers, oligomers, and fibrils and confirm the effects of 1,4-NQ derivatives **YQ-001**, **YQ-002**, **YQ-003**, **YQ-004**, **YQ-010**, **YQ-011**, **YQ-019**, **YQ-029**, **YQ-030**, **YQ-031**, **YQ-032**, **YQ-033**, **YQ-034**, and **YQ-036** on Aβ aggregation. Due to the metastable nature of oligomers (oligomers dynamically disaggregate into monomers and aggregate into fibrils over time) PICUP chemistry is a necessary procedure that covalently stabilizes oligomers to enable clear visualization of the different distributions of Aβ in SDS-PAGE.[18] The SDS-PAGE analysis results revealed that none of the compounds have inhibited aggregation of Aβ (Figure 3A) or reduced Aβ fibrils (Figure 3B), which is inconsistent with the previous ThT assay results. We determined that all 41 1,4-NQ derivatives did not regulate Aβ aggregate formation and that the ThT assay may have produced false-positive data.

Fluorescence Spectral Scan of 1,4-NQ Derivatives. Given the conflicting results of the ThT assay and SDS-PAGE analysis, we suspected that the 1,4-NQ derivatives may be fluorescent and thus affected the ThT assay results of each sample. To verify our hypothesis, we conducted fluorescence spectroscopy to measure the fluorescent property of the selected 14 compounds with and without presence of Aβ aggregates. We recorded the absorbance spectra of the selected 14 of the 1,4-NQ derivatives to obtain the fluorescent excitation wavelength, or the highest peak of the spectrum (Figure S2A). To obtain the emission point, we measured the fluorescence emission spectra by exciting each compound according to their excitation wavelengths respectively (Figure S2B). The spectral activities of the compounds overlap with the range of the ThT dye, which supports our hypothesis that these compounds may have induced false positives in ThT assay due to fluorescence interference.[19] Afterward, we selected nine candidates suitable for fluorescence detection of Aβ aggregates in vitro and ex vivo: **YQ-002**, **YQ-003**, **YQ-004**, **YQ-030**, **YQ-031**, **YQ-032**, **YQ-033**, **YQ-034**, and **YQ-036**.

If our fluorescent compounds interact with Aβ, there could be a noticeable change in the fluorescence spectrum or intensity. The selected nine YQ compounds were added to Aβ monomers or Aβ aggregates. Of the nine compounds, **YQ-002**, **YQ-003**, **YQ-030**, and **YQ-036** have increased fluorescence when mixed with Aβ monomers or aggregates (Figure 4A). When in the presence of Aβ monomers or aggregates, **YQ-030** produces a drastic increase in fluorescence by nearly 2-fold at its emission peak, whereas **YQ-002**, **YQ-003**, and **YQ-036** did not show a significant increase fluorescence intensity at their emission peaks. The compounds **YQ-002** and **YQ-003** exhibited higher fluorescence intensities when in the presence of Aβ monomers and aggregates, while **YQ-036** enhanced fluorescence in the presence of Aβ aggregates between specific spectrum regions (**YQ-002**: 480−670 nm, **YQ-003**: 580−700 nm, **YQ-036**: 500−680 nm). Among these four compounds,

DOI: 10.1021/acschemneuro.9b00093
ACS Chem. Neurosci. XXXX, XXX, XXX−XXX

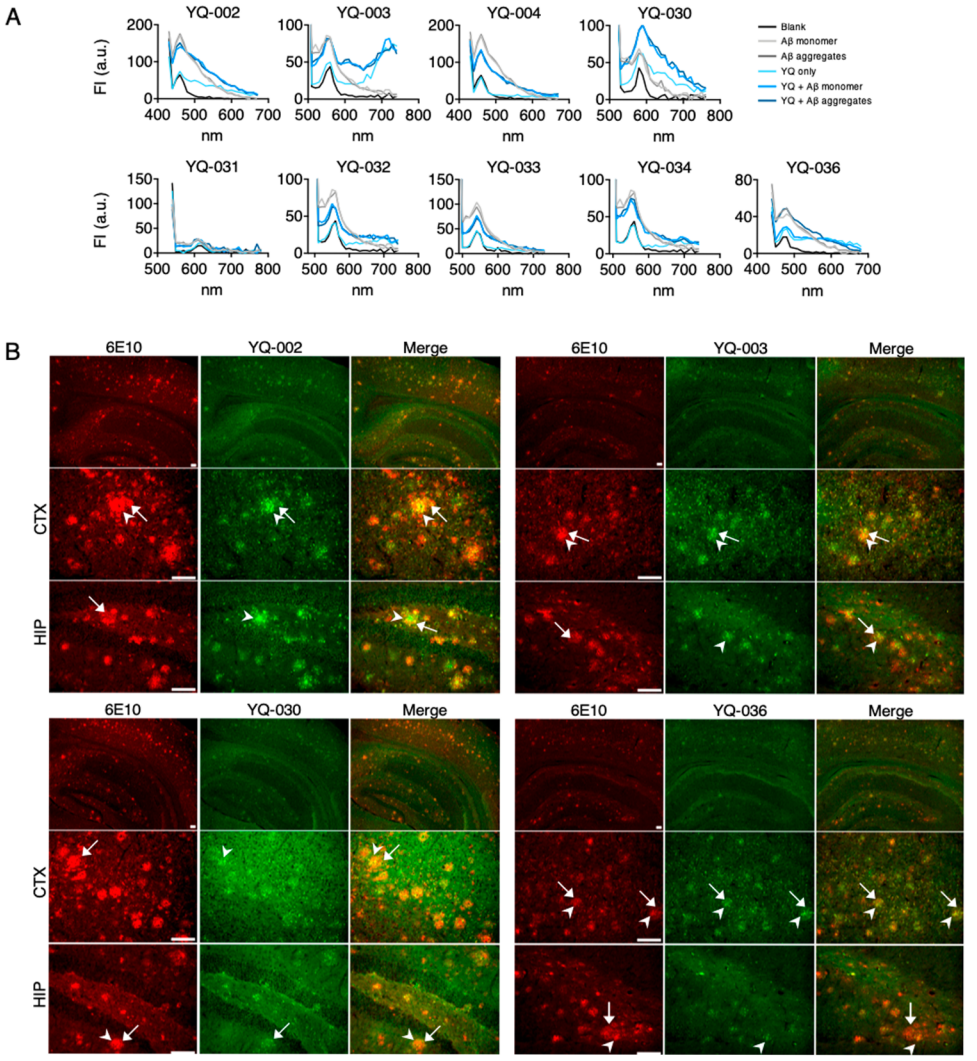

Figure 4. Fluorescence spectral scan of selected 1,4-NQ derivatives and histochemistry of AD model mouse brain tissue by selected 1,4-NQ derivatives. (A) Emission spectra of YQ compounds (50 μM) with synthesized Aβ42 (50 μM) in 3:1 ratio were measured by using their respective excitation wavelengths to show the fluorescence intensity (FI) between two ranges. The excitation wavelengths for the compounds are as follows: **YQ-002**, 400 nm; **YQ-003**, 470 nm; **YQ-004**, 400 nm; **YQ-030**, 490 nm; **YQ-031**, 510 nm; **YQ-032**, 470 nm; **YQ-033**, 460 nm; **YQ-034**, 470 nm; **YQ-036**, 410 nm. These graphs contain four control groups (Aβ monomer, Aβ aggregates, blank, YQ) and two experimental groups (YQ + Aβ monomer, YQ + Aβ aggregates). Spectra of all samples were measured using an Infinite 200 PRO plate reader. See also Figure S2. (B) Histochemistry of aged male APP/PS1 double transgenic mouse brains was conducted by staining brain slices with 6E10 or YQ compounds (**YQ-002**, **YQ-003**, **YQ-030**, and **YQ-036**). The images of 6E10 and YQ compounds were merged to confirm that both demonstrate colocalization on both diffuse (arrow) and dense-core (arrowhead) Aβ42 plaques. Scale bars = 100 μm.

YQ-003 is the only compound that enhances fluorescence by up to 50-fold when emission is collected from 680 to 750 nm. Altogether, we found four compounds that enhance or alter their fluorescence properties in the presence of Aβ aggregates. The fluorescent enhancements of 1,4-NQ derivatives in the presence of Aβ imply that these compounds may have potential to be amyloid imaging agents.

Histochemistry of AD Model Mouse Brain Tissue by 1,4-NQ Derivatives. To ascertain whether these 1,4-NQ derivatives can detect Aβ plaques ex vivo, we conducted histochemistry on fixed mouse brain tissues of aged APP/PS1 double transgenic AD mouse models, which are reported to develop amyloid plaques in the cortex at around the age of 6months.[20] We performed brain staining using four YQ compounds and anti-Aβ monoclonal antibody 6E10. Thioflavin S only labels dense-core plaques whereas 6E10 can stain both dense-core and diffuse plaques. We observed that these 1,4-NQ derivatives are colocalized with 6E10 on plaques containing dense cores with or without surrounding diffuse Aβ assemlies in the hippocampal and cortical regions (Figure 4B). Of these compounds, **YQ-002**, **YQ-003**, and **YQ-036** were deemed as promising imaging agents for staining Aβ plaques in APP/PS1 mouse brains as they demonstrate the highest fluorescence contrast and overlap with 6E10 more effectively than **YQ-030** does.

Molecular Docking Models of the Fluorescent Compounds to Aβ. The molecular docking models for **YQ-002**, **YQ-003**, **YQ-030**, and **YQ-036** were investigated due to their increased fluorescence when mixed with Aβ and their histochemical plaque-staining function. Since there was no prior knowledge on binding sites for the new compounds, we first performed an exhaustive global (low-resolution) docking conformation search by using PatchDock software[21] to predict potential binding pockets in Aβ. As a result, center of mass

DOI: 10.1021/acschemneuro.9b00093
ACS Chem. Neurosci. XXXX, XXX, XXX−XXX

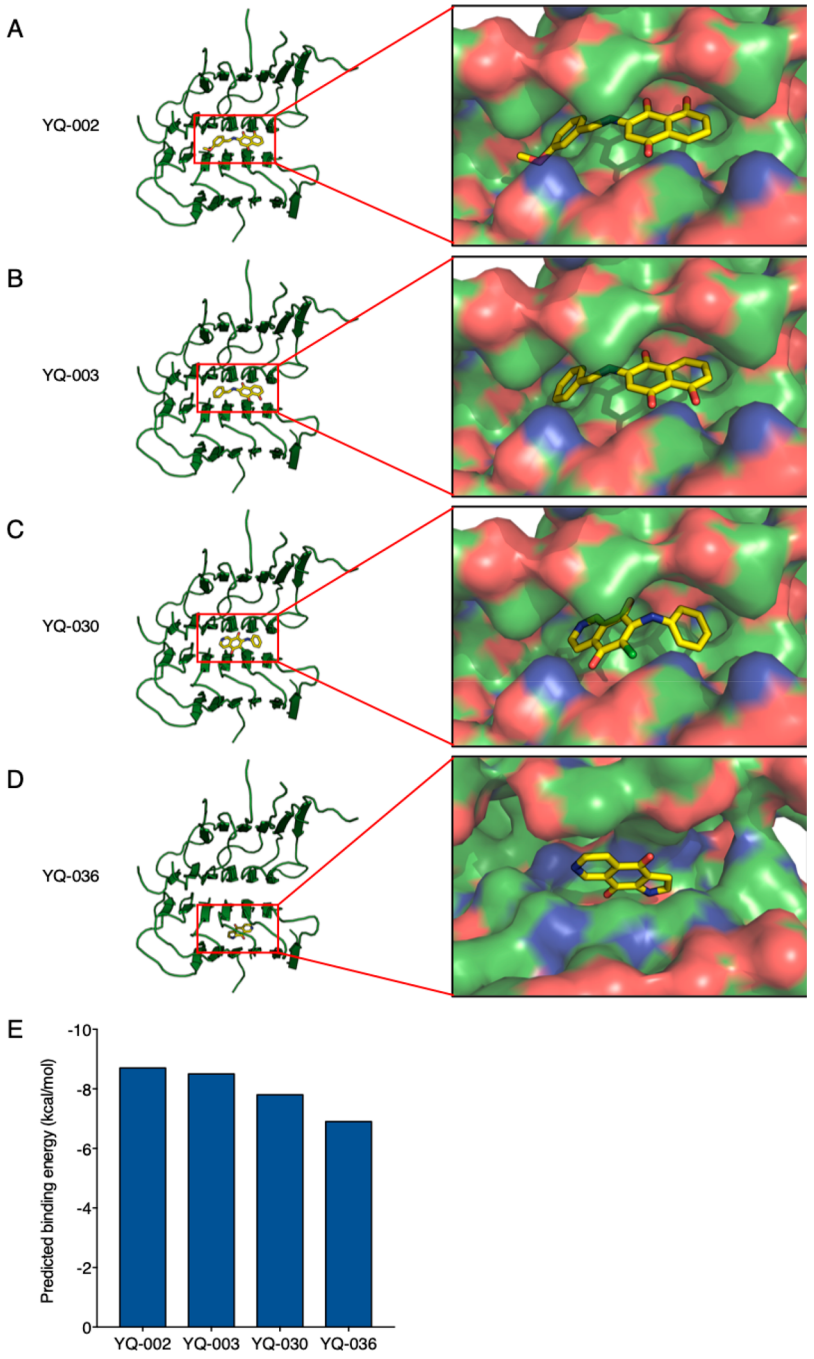

Figure 5. Molecular docking models for selected 1,4-NQ derivatives. Molecular docking models of (A) **YQ-002**, (B) **YQ-003**, (C) **YQ-030**, and (D) **YQ-036** are presented by docking simulations using PatchDock and Autodock vina. To clarify the binding modes, the zoomed binding pocket in Aβ aggregates is represented by surface and the docked ligands (carbon in yellow) are shown by sticks. (E) Predicted binding energy values by Autodock vina of **YQ-002**, **YQ-003**, **YQ-030**, and **YQ-036**. All figures were created with PyMOL software.

coordinates of the bound ligands in the top 100 docking conformations were used as an initiate position for the subsequent docking simulation by Autodock vina to generate more refined docking models.[22] After the docking refinements, the docking conformation with the lowest binding energy was considered as the final binding model for each fluorescent compound (Figure 5A–D).

All the compounds (Figure 5A–C) except **YQ-036** (Figure 5D) were docked into the same binding pocket formed between β-sheets. The predicted binding energy values by Autodock vina were −8.7, −8.5, −7.8, and −6.9 kcal/mol for **YQ-002**, **YQ-003**, **YQ-030**, and **YQ-036**, respectively (Figure 5E). **YQ-002** showed the lowest binding energy, and, in the docking model of **YQ-002**, the aromatic rings fit into the hydrophobic pocket formed by Ile31 and Val40 (Figure 5A and E). Similar interactions were also found in **YQ-003** and **YQ-030** docking models, but **YQ-036** was docked into the opposite binding site inside the β-strands of Aβ with the least predicted binding affinity. All the docking models suggest that the four fluorescent compounds bind to Aβ with favorable hydrophobic interactions and high shape complementarity.

DOI: 10.1021/acschemneuro.9b00093
ACS Chem. Neurosci. XXXX, XXX, XXX−XXX

PAMPA for Prediction of Blood-Brain Barrier Permeability of 1,4-NQ Derivatives. The ability to cross the BBB is one of the main criteria required for amyloid imaging agent candidates. PAMPA determines the permeability of compounds by passively diffusing compounds from donor plates across a BBB-like artificial lipid membrane into acceptor plates. The UV−vis spectra of the reference compound standard, acceptor, and donor plates were measured and effective permeability (P_e) of the compounds were calculated by the PAMPA Explorer software (pION Inc.). Compounds are classified as BBB permeable (CNS+) or BBB impermeable (CNS−) based on their measured effective permeability ($-\log P_e$). In accordance with previous reports, $-\log P_e$ values of compounds less than 5.4 are classified as CNS+, and CNS− for values greater than 5.7.[23] The $-\log P_e$ values of **YQ-002**, **YQ-003**, **YQ-030**, and **YQ-036** are 4.2, 4.1, 4.1, and 4.6, respectively, suggesting that all compounds are predicted to be highly permeable (Table 1).

Table 1. PAMPA for Prediction of Blood-Brain Barrier Permeability of Selected 1,4-NQ Derivatives[a]

compd	P_e (10^{-6} cm s^{-1})	$-\log P_e$	CNS prediction
theophylline	4.4	5.4	CNS±
lidocaine	82.9	4.1	CNS+
progesterone	111.0	4.0	CNS+
YQ-002	69.9	4.2	CNS+
YQ-003	73.6	4.1	CNS+
YQ-030	72.7	4.1	CNS+
YQ-036	26.2	4.6	CNS+

[a]The UV−vis spectra of the acceptor and donor plates were measured after the compounds passively diffused across a BBB-like membrane. Compounds with $-\log P_e$ below values 5.4 are regarded as CNS+, and higher than 5.7 are regarded as CNS−. Theophylline is a negative control, and lidocaine and progesterone are positive controls.

Surface Plasmon Resonance Analysis to Confirm Aβ Binding Property. To confirm direct interaction between 1,4-NQs and Aβ aggregates, surface plasmon resonance analysis was employed to investigate biomolecular binding kinetics using a Biacore T200 system. In accordance with the positive histochemistry results, we selected **YQ-002** as the candidate for this assay. Aβ42 aggregates were fixed onto a CM5 sensor chip by amine coupling, and **YQ-002** in various concentrations (from 100 to 500 μM) was passed through the chip surface as an analyte. During the dissociating phase, **YQ-002** was found to not dissociate from the Aβ aggregates, indicating strong binding to the target; thus, we conducted single-cycle kinetics analysis instead of the common multicycle kinetic analysis. The binding response continuously increased relative to the concentration of **YQ-002** (Figure S3), suggesting that **YQ-002** directly binds to immobilized Aβ aggregates in a dose-dependent manner. The result is consistent to the docking model results with the lowest binding energy of the compound. The K_D value could not be calculated properly due to the heterogeneous nature of immobilized Aβ aggregates.[24]

DISCUSSION

Our study reveals that 1,4-NQ derivatives can exhibit fluorescence when bound to Aβ aggregates ex vivo. Considering that dense-core plaques are highly correlated with pathogenesis of AD and diffuse plaques are the early manifestations of dense-core plaques, detection of both forms of Aβ plaques in the brain will significantly contribute to clinical diagnosis of early AD.[25−27] The compound **YQ-003** shows the most promising results as it shows diffuse and dense-core Aβ plaques in APP/PS1 AD mouse model brain sections and can penetrate through the BBB based on PAMPA analysis. **YQ-003** also enhances fluorescence by 50-fold when its emission is collected from 680 to 750 nm; considering that biological tissues have lower absorption of NIR light and NIR enables higher signal-to-background ratio than visible wavelengths, the NIR emission property of **YQ-003** is very suitable for an in vivo AD imaging agent candidate.[28] The surface plasmon resonance analyses showed that the binding property of **YQ-002** is unfavorable for clinical applications due to its low dissociation rate; current imaging agents are labeled with radioisotopes and must be cleared out from the brain within a short time frame to minimize risks of radiation.[29,30] However, the strong affinity to Aβ aggregates suggest that **YQ-003** or other derivatives of the 1,4-NQ scaffold could have potential as amyloid imaging candidates and will require further studies.

Further investigation is also warranted to in vivo studies including micro positron emission tomography of AD mouse model, pharmacokinetic profiling, and isotope labeling kinetics.[31] We hypothesized that these compounds interfered with ThT by preventing it from binding to the β-sheets of Aβ aggregates or by altering its fluorescence intensity due to overlapping spectral activity. The overall binding mechanism of ThT consists of the chemical dye approaching the surfaces of cross-β-sheets formed by continuous chains of tyrosine and leucine before undertaking a twisted, chiral conformation to bind to the cross-β-sheets.[32] Considering that the wavelengths of several 1,4-NQ derivatives overlap with ThT and the compounds fluoresce in the presence of Aβ, our evidence suggests that the dramatic decrease in fluorescence intensity from ThT assay could be due to the 1,4-NQ derivatives directly competing with ThT for the same binding sites on the β-sheets.[17,19] To further validate this claim, additional biochemical, biophysical, and structural investigations must be carried out in follow up studies to explicate the underlying mechanisms of 1,4-NQ derivatives on Aβ.

Current clinically approved amyloid imaging agents were developed based on the chemical structures of the common Aβ histologic dyes ThT and Congo Red, both of which consisting of amyloid-binding benzothiazole moieties.[33,34] Given that these imaging agents exhibit low binding affinity toward diffuse plaques, our study suggests that 1,4-NQ can be used as a novel scaffold that can target both dense-core and diffuse plaques to develop imaging agents for early AD patients. Overall, our data indicates that 1,4-NQ scaffold can bind to Aβ and serve as a basis for future designs of drug and diagnostic tool development for AD.

METHODS

Chemical Syntheses of 1,4-Naphthoquinone Derivatives. The synthetic procedure for **YQ-001** and **YQ-002** was adapted from

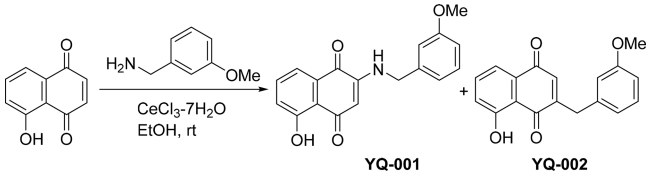

DOI: 10.1021/acschemneuro.9b00093
ACS Chem. Neurosci. XXXX, XXX, XXX−XXX

the literature procedure.[35,36] To a stirred mixture of 5-hydroxy-1,4-naphthoquinone (45 mg, 0.258 mmol, 1 equiv) and $CeCl_3{\cdot}7H_2O$ (4.8 mg, 0.05 equiv) in EtOH (2 mL) was added 3-methoxybenzylamine (40 μL, 1.2 equiv) at rt. After being stirred at rt for 2 h, the reaction mixture was concentrated in vacuo, suspended in water, suction-filtered, and dried. The resulting solid was purified by silica gel column chromatography (hexanes/ethyl acetate/dichloromethane = 20:1:2 to 10:1:2) to give **YQ-001** (upper spot) and **YQ-002** (lower spot). The following compounds (**YQ-003**, **YQ-004**, **YQ-005**, **YQ-006**, **YQ-007**, **YQ-008**, **YQ-009**, **YQ-010**, **YQ-011**, **YQ-012**, **YQ-013**, **YQ-014**, **YQ-015**, **YQ-016**, **YQ-017**, **YQ-018**, **YQ-019**, **YQ-020**, **YQ-021**, **YQ-022**, **YQ-023**, **YQ-024**, **YQ-032**, **YQ-033**, **YQ-034**, and **YQ-035**) were prepared by the same procedure used for the synthesis of **YQ-001** and **002**. Isoquinoline-5,8-dione was synthesized by following the literature procedure.[37,38]

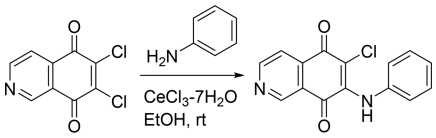

YQ-025

The synthetic procedure for **YQ-025** was adapted from the literature procedure.[39,40] To a stirred mixture of 6,7-dichloroisoquinoline-5,8-dione (20 mg, 0.088 mmol, 1 equiv) and $CeCl_3{\cdot}7H_2O$ (1.63 mg, 0.05 equiv) in EtOH (1.2 mL) was added aniline (12 μL, 1.5 equiv) at rt. After being stirred at rt for 3 h, the reaction mixture was concentrated in vacuo and purified by silica gel column chromatography (hexanes/ethyl acetate/dichloromethane = 3:1:2 to dichloromethane only to dichloromethane/MeOH = 10:1) to give **YQ-025**. 6,7-Dichloroisoquinoline-5,8-dione was prepared by following the known procedure.[41] The following compounds (**YQ-026**, **YQ-027**, **YQ-028**, **YQ-029**, **YQ-030**, and **YQ-031**) were prepared by the same procedure for the synthesis of **YQ-025**.

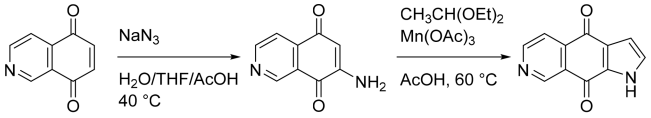

7-aminoisoquinoline-5,8-dione **YQ-036**

The synthetic procedure for **YQ-036** was adapted from the literature procedure.[42,43] To a stirred mixture of isoquinoline-5,8-dione (94 mg, 0.59 mmol, 1 equiv) in THF/AcOH (1/1, 3 mL) was added a solution of NaN_3 (50 mg, 0.77 mmol, 1.3 equiv) in H_2O (1.5 mL) at rt. After being stirred at 40 °C for 3 h, the reaction mixture was concentrated under reduced pressure, diluted with H_2O, and extracted with CH_2Cl_2. The organic layer was washed with aq. $NaHCO_3$, dried over $MgSO_4$, and concentrated in vacuo to give the crude residue, which was used for the next step without further purification. A mixture of 7-aminoisoquinoline-5,8-dione (65 mg, 0.373 mmol, 1 equiv), acetaldehyde diethyl acetal (218 μL, 1.53 mmol, 4.1 equiv), and $Mn(OAc)_3$ (500 mg, 1.866 mmol, 5 equiv) in AcOH (6 mL) was heated at 60 °C for 3 h. The reaction mixture was concentrated under reduced pressure, diluted with H_2O, and extracted with ethyl acetate. The organic layer was washed with aq. $NaHCO_3$, dried over $MgSO_4$, and concentrated in vacuo to give **YQ-036**.

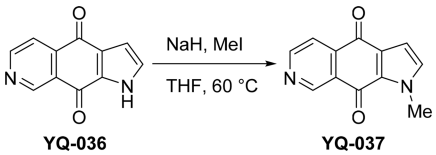

YQ-036 **YQ-037**

The synthetic procedure for **YQ-037** was adapted from the literature procedure.[43] To a stirred mixture of **YQ-036** (20 mg, 0.1 mmol, 1 equiv) in THF (1.5 mL) were added 60% NaH (12 mg, 0.3 mmol, 3 equiv) and MeI (18 μL, 0.3 mmol, 3 equiv) at 0 °C. After being stirred at 60 °C for 6 h, the reaction mixture was quenched with H_2O, concentrated under reduced pressure, diluted with H_2O, and extracted with CH_2Cl_2. The organic layer was dried over $MgSO_4$ and concentrated in vacuo to give the crude residue, which was purified by silica gel column chromatography (hexanes/ethyl acetate/dichloromethane = 7:1:2 to 1:1:1) to give **YQ-037**.

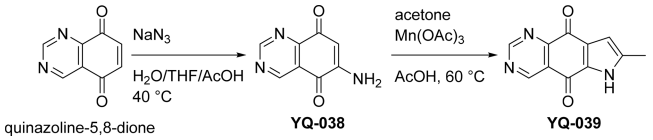

quinazoline-5,8-dione **YQ-038** **YQ-039**

Compounds **YQ-038** and **YQ-039** were synthesized by following the procedures for the synthesis of **YQ-036**. Quinazoline-5,8-dione was prepared by following the literature procedure.[44]

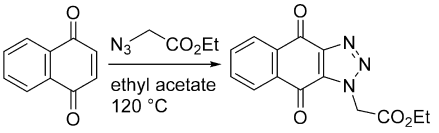

YQ-040

The synthetic procedure for **YQ-040** was adapted from the literature procedure.[45] A mixture of 1,4-naphthoquinone (50 mg, 0.316 mmol, 1 equiv) and ethyl azidoacetate (102 mg, 0.79 mmol, 2.5 equiv) was heated at 120 °C for 24 h. After evaporation of the solvent, the residue was purified by silica gel column chromatography (hexanes/ethyl acetate/dichloromethane = 20:1:2 to 10:1:2 to 5:1:2 to 1:1:1) to give **YQ-040**. **YQ-041** was synthesized by following the same procedure for the synthesis of **YQ-040**.

*5-Hydroxy-2-((3-methoxybenzyl)amino)naphthalene-1,4-dione (**YQ-001**).* Orange solid, mp: 114.8–118.9 °C; ^{1}H NMR (400 MHz, $CDCl_3$) δ 13.0 (s, 1H), 7.6 (d, J = 7.2 Hz, 1H), 7.48 (t, J = 7.8 Hz, 1H), 7.32–7.24 (m, 3H), 6.90–6.84 (m, 3H), 6.39 (s, 1H), 5.67 (s, 1H), 4.37 (d, J = 5.2 Hz, 2H), 3.82 (s, 3H); ^{13}C NMR (100 MHz, $CDCl_3$) δ 189.21, 181.17, 161.23, 160.25, 148.53, 137.18, 134.14, 130.56, 130.30, 126.10, 119.88, 119.23, 114.98, 113.53, 113.50, 100.85, 55.43, 46.96; HRMS (ESI-QTOF) m/z [M + H]$^+$ calcd for $C_{18}H_{16}NO_4$ 310.1074, found 310.1081.

*8-Hydroxy-2-((3-methoxybenzyl)amino)naphthalene-1,4-dione (**YQ-002**).* Orange solid, mp: 169.6–170.3 °C; ^{1}H NMR (400 MHz, $CDCl_3$) δ 11.53 (s, 1H), 7.61(d, J = 4.4 Hz, 2H), 7.30 (t, J = 8.0 Hz, 1H), 7.14 (t, J = 4.8 Hz, 1H), 6.90 (d, J = 7.2 Hz, 1H), 6.88–6.84 (m, 2H), 6.18 (s, 1H), 5.75 (s, 1H), 4.35 (d, J = 5.6 Hz, 2H), 3.82 (s, 3H); ^{13}C NMR (100 MHz, $CDCl_3$) δ 186.15, 182.47, 161.82, 160.27, 147.63, 137.85, 137.41, 133.54, 130.30, 122.48, 119.91, 118.95, 114.20, 113.53, 113.50, 102.54, 55.45, 46.95; HRMS (ESI-QTOF) m/z [M + H]$^+$ calcd for $C_{18}H_{16}NO_4$ 310.1074, found 310.1074.

*2-(Benzylamino)-5-hydroxynaphthalene-1,4-dione (**YQ-003**).* Red solid, mp: 150–151.3 °C; ^{1}H NMR (400 MHz, $CDCl_3$) δ 12.99 (s, 1H), 7.61 (d, J = 7.6 Hz, 1H), 7.48 (t, J = 7.8 Hz, 1H), 7.41–7.30 (m, 6H), 7.24 (s, 1H), 7.41–7.34 (m, 5H), 7.24 (s, 1H), 6.37 (s, 1H), 5.69 (s, 1H), 4.39 (d, J = 6.0 Hz, 2H); ^{13}C NMR (100 MHz, $CDCl_3$) δ 189.25, 181.23, 161.27, 148.54, 147.52, 135.62, 134.17, 130.60, 129.25, 128.44, 127.79, 126.14, 119.26, 100.83, 47.06; HRMS (ESI-QTOF) m/z [M + H]$^+$ calcd for $C_{17}H_{14}NO_3$ 280.0968, found 280.0970.

*2-(Benzylamino)-8-hydroxynaphthalene-1,4-dione (**YQ-004**).* Red solid, mp: 207.8–208.2 °C; ^{1}H NMR (400 MHz, $CDCl_3$) δ 11.53 (s, 1H), 7.62 (d, J = 4.4 Hz, 2H), 7.41–7.31 (m, 5H), 7.15 (t, J = 4.8 Hz, 1H), 6.19 (s, 1H), 5.76 (s, 1H), 4.38 (d, J = 5.6 Hz, 2H); ^{13}C NMR (100 MHz, $CDCl_3$) δ 186.16, 182.46, 161.82, 147.63, 137.86, 135.85, 133.55, 129.22, 128.38, 127.78, 122.48, 118.95, 114.20, 102.49, 47.00; HRMS (ESI-QTOF) m/z [M + H]$^+$ calcd for $C_{17}H_{14}NO_3$ 280.0968, found 280.0966.

*8-Hydroxy-2-((4-nitrophenyl)amino)naphthalene-1,4-dione (**YQ-005**).* Red solid, mp: 332–333 °C; ^{1}H NMR (400 MHz, DMSO-d_6) δ 11.5 (s, 1H), 9.67 (s, 1H), 8.28 (d, J = 8.8 Hz, 1H), 7.77 (t, J = 8.0 Hz, 1H), 7.67 (d, J = 8.8 Hz, 2H), 7,50 (d, J = 7.2 Hz, 1H), 7.31

DOI: 10.1021/acschemneuro.9b00093
ACS Chem. Neurosci. XXXX, XXX, XXX–XXX

(d, J = 8.4 Hz, 1H), 6.46 (s, 1H); ^{13}C NMR (100 MHz, DMSO-d_6) δ 160.86, 137.94, 125.58, 123.21, 122.52, 118.19, 106.78; HRMS (ESI-QTOF) m/z [M + H]$^+$ calcd for $C_{16}H_{11}N_2O_5$ 311.0662, found 311.0663.

*8-Hydroxy-2-(p-tolylamino)naphthalene-1,4-dione (**YQ-006**).* Red solid, mp: 193.4−196.4 °C; ^{1}H NMR (400 MHz, $CDCl_3$) δ 11.57 (s, 1H), 7.67−7.62 (m, 2H), 7.47 (s, 1H), 7.23 (d, J = 8.0 Hz, 2H), 7.20−7.15 (m, 3H), 6.31 (s, 1H), 2.37 (s, 3H); ^{13}C NMR (100 MHz, $CDCl_3$) δ 186.39, 183.19, 161.87, 145.08, 137.97, 136.05, 134.61, 133.34, 130.44, 123.02, 122.68, 118.88, 114.17, 103.70, 21.16; HRMS (ESI-QTOF) m/z [M + H]$^+$ calcd for $C_{17}H_{14}NO_3$ 280.0968, found 280.0968.

*2-((4-Bromophenyl)amino)-8-hydroxynaphthalene-1,4-dione (**YQ-007**).* Brown solid, mp: 225−227 °C; ^{1}H NMR (400 MHz, DMSO-d_6) δ 11.52 (s, 1H), 9.32 (s, 1H), 7.74 (t, J = 8.0 Hz, 1H), 7.62 (d, J = 8.8 Hz, 2H), 7.47 (d, J = 8.8 Hz, 1H), 7.36 (d, J = 8.8 Hz, 2H), 7.27 (d, J = 8.4 Hz, 1H), 6.08 (s, 1H); ^{13}C NMR (100 MHz, DMSO-d_6) δ 185.78, 182.45, 160.89, 146.25, 137.97, 137.92, 133.26, 132.59, 126.05, 122.80, 118.07, 117.68, 114.74, 103.25; HRMS (ESI-QTOF) m/z [M + H]$^+$ calcd for $C_{16}H_{11}BrNO_3$ 343.9917, found 343.9917.

*Ethyl 3-((8-hydroxy-1,4-dioxo-1,4-dihydronaphthalen-2-yl)-amino)benzoate (**YQ-008**).* Brown solid, mp: 169.6−172 °C; ^{1}H NMR (400 MHz, $CDCl_3$) δ 11.53 (s, 1H), 7.91 (d, J = 8.8 Hz, 2H), 7.68−7.63 (m, 2H), 7.57 (s, 1H), 7.53−7.47 (m, 2H), 7.20 (dd, J = 2, 2.2 Hz, 1H), 6.36 (s, 1H), 4.41 (q, J = 7.2 Hz, 2H), 1.41 (t, J = 7.2 Hz, 3H); ^{13}C NMR (100 MHz, $CDCl_3$) δ 186.01, 183.23, 165.73, 161.90, 144.62, 138.05, 137.63, 133.08, 132.42, 129.94, 126.92, 123.94, 122.93, 119.01, 114.05, 104.48, 61.59, 29.83, 14.45; HRMS (ESI-QTOF) m/z [M + H]$^+$ calcd for $C_{19}H_{16}NO_5$ 338.1023, found 338.1024.

*2-((4-Chlorophenyl)amino)-8-hydroxynaphthalene-1,4-dione (**YQ-009**).* Brown solid, mp: 228−229 °C; ^{1}H NMR (400 MHz, DMSO-d_6) δ 11.48 (s, 1H), 9.29 (s, 1H), 7.71 (t, J = 8.0 Hz, 1H), 7.41−7.37 (m, 5H), 7.34 (d, J = 8.4 Hz, 1H), 6.03 (s, 1H); ^{13}C NMR (100 MHz, DMSO-d_6) δ 185.79, 160.88, 146.37, 137.98, 129.68, 125.78, 122.79, 118.07, 103.16; HRMS (ESI-QTOF) m/z [M + H]$^+$ calcd for $C_{16}H_{11}ClNO_3$ 300.0422, found 300.0423.

*8-Hydroxy-2-(phenylamino)naphthalene-1,4-dione (**YQ-010**).* Orange solid, mp: 204−206 °C; ^{1}H NMR (400 MHz, $CDCl_3$) δ 11.57 (s, 1H), 7.66−7.63 (m, 2H), 7.53 (s, 1H), 7.44 (t, J = 7.6 Hz, 2H), 7.28 (d, J = 7.6 Hz, 2H), 7.24−7.19 (m, 2H), 6.38 (s, 1H); ^{13}C NMR (100 MHz, $CDCl_3$) δ 186.30, 183.29, 161.90, 144.81, 138.01, 137.31, 133.24, 129.91, 126.02, 122.94, 122.80, 118.93, 114.15, 104.08; HRMS (ESI-QTOF) m/z [M + H]$^+$ calcd for $C_{16}H_{12}NO_3$ 266.0812, found 266.0811.

*8-Hydroxy-2-((3,4,5-trimethoxyphenyl)amino)naphthalene-1,4-dione (**YQ-011**).* Brown solid, mp: 167.1−168.9 °C; ^{1}H NMR (400 MHz, $CDCl_3$) δ 11.55 (s, 1H), 7.68−7.63 (m, 2H), 7.42 (s, 1H), 7.20 (dd, J = 2.4, 6.8 Hz, 1H), 6.49 (s, 2H), 6.30 (s, 1H), 3.87 (s, 6H), 3.86 (s, 3H); ^{13}C NMR (100 MHz, $CDCl_3$) δ 186.21, 183.17, 161.89, 154.13, 145.23, 138.06, 136.37, 133.25, 133.00, 122.79, 118.97, 114.09, 104.07, 101.04, 61.19, 56.46; HRMS (ESI-QTOF) m/z [M + H]$^+$ calcd for $C_{19}H_{18}NO_6$ 356.1129, found 356.1130.

*7-((4-Methoxyphenyl)amino)isoquinoline-5,8-dione (**YQ-012**).* Black solid, mp: 227.6−228 °C; ^{1}H NMR (400 MHz, $CDCl_3$) δ 9.33 (s, 1H), 9.04 (d, J = 4.8 Hz, 1H), 7.91 (d, J = 4.8 Hz, 1H), 7.51 (s, 1H), 7.20 (d, J = 8.8 Hz, 2H), 6.97 (d, J = 8.8 Hz, 2H), 6.29 (s, 1H), 3.84 (s, 1H); ^{13}C NMR (100 MHz, $CDCl_3$) δ 181.95, 181.73, 158.26, 156.59, 148.20, 145.87, 139.02, 129.39, 125.26, 124.32, 118.95, 115.18, 103.01, 55.73; HRMS (ESI-QTOF) m/z [M + H]$^+$ calcd for $C_{16}H_{13}N_2O_3$ 281.0921, found 281.0920.

*2-((4-Fluorophenyl)amino)-8-hydroxynaphthalene-1,4-dione (**YQ-013**).* Red solid, mp: 235.8−236.7 °C; ^{1}H NMR (400 MHz, $CDCl_3$) δ 8.12 (t, J = 7.2 Hz, 2H), 7.77 (t, J = 7.2 Hz, 1H), 7.68 (t, J = 7.4 Hz, 1H), 7.45 (s, 1H), 7.24 (s, 2H), 7.13 (t, J = 7.8 Hz, 2H), 6.26 (s, 1H); ^{13}C NMR (100 MHz, $CDCl_3$) δ 183.98, 182.09, 145.42, 135.13, 133.44, 132.56, 130.47, 126.68, 126.36, 125.19, 125.11, 116.90, 116.67, 103.26; HRMS (ESI-QTOF) m/z [M + H]$^+$ calcd for $C_{16}H_{11}FNO_2$ 268.0768, found 268.0768.

*2-(p-Tolylamino)naphthalene-1,4-dione (**YQ-014**).* Pink solid, mp: 192.4−195.1 °C; ^{1}H NMR (400 MHz, CDCl3) δ 8.11 (t, J = 6.2 Hz, 2H), 7.76 (t, J = 7.6 Hz, 1H), 7.66 (t, J = 7.2 Hz, 1H), 7.51 (s, 1H), 7.25−7.13 (m, 4H), 6.36 (s, 1H), 2.37 (s, 3H); 13C NMR (100 MHz, CDCl3) δ 184.00, 182.30, 145.16, 135.79, 135.04, 134.87, 133.46, 132.40, 130.54, 130.38, 126.63, 126.29, 122.87, 103.17, 21.15; HRMS (ESI-QTOF) m/z [M + H]+ calcd for $C_{17}H_{14}NO_2$ 264.1019, found 264.1015.

*2-((4-Bromophenyl)amino)naphthalene-1,4-dione (**YQ-015**).* Red solid, mp: 269.9−271.5 °C; ^{1}H NMR (400 MHz, DMSO-d_6) δ 9.30 (s, 1H), 8.07 (d, J = 7.6 Hz, 1H), 7.96 (d, J = 7.6 Hz, 1H), 7.87 (t, J = 7.6 Hz, 1H), 7.80 (t, J = 7.8 Hz, 1H), 7.62 (d, J = 8.4 Hz, 2H), 7.37 (d, J = 8.4 Hz, 2H) 6.15 (s, 1H); ^{13}C NMR (100 MHz, DMSO-d_6) δ 82.74, 181.46, 145.79, 137.63, 134.94, 132.77, 132.49, 132.16, 130.44, 126.19, 125.48, 125.32, 117.11, 102.66; HRMS (ESI-QTOF) m/z [M + H]$^+$ calcd for $C_{16}H_{11}BrNO_2$ 327.9968, found 327.9968.

*2-((4-Chlorophenyl)amino)-8-hydroxynaphthalene-1,4-dione (**YQ-016**).* Red solid, mp: 267.8−270 °C; ^{1}H NMR (400 MHz, DMSO-d_6) δ 9.30 (s, 1H), 8.07 (d, J = 7.2 Hz, 1H), 7.96 (d, J = 7.2 Hz, 1H), 7.87 (t, J = 7.4 Hz, 1H), 7.80 (t, J = 7.6 Hz, 1H), 7.49 (d, J = 8.4 Hz, 2H), 7.43 (d, J = 7.6 Hz, 2H), 6.13 (s, 1H); ^{13}C NMR (100 MHz, DMSO-d_6) δ 182.72, 181.46, 145.90, 137.19, 134.94, 132.76, 132.50, 130.44, 129.25, 128.96, 126.19, 125.32, 125.20, 102.56; HRMS (ESI-QTOF) m/z [M + H]$^+$ calcd for $C_{16}H_{11}ClNO_2$ 284.0473, found 284.0472.

*Ethyl 3-((1,4-dioxo-1,4-dihydronaphthalen-2-yl)amino)benzoate (**YQ-017**).* Orange solid, mp: 138−194 °C; ^{1}H NMR (400 MHz, DMSO-d_6) δ 9.39 (s, 1H), 8.07 (d, J = 7.6 Hz, 1H), 7.95 (d, J = 6.0 Hz, 2H), 7.86 (t, J = 7.4 Hz, 1H), 7.79 (t, J = 7.8 Hz, 2H), 7.68 (d, J = 7.6 Hz, 1H), 7.59 (t, J = 7.8 Hz, 1H), 6.12 (s, 1H), 4.33 (q, J = 6.8 Hz, 2H), 1.33 (t, J = 7.0 Hz, 3H); ^{13}C NMR (100 MHz, DMSO-d_6) δ 182.77, 181.35, 165.25, 146.07, 138.68, 134.89, 132.75, 132.47, 130.99, 130.44, 129.81, 128.11, 126.17, 125.59, 125.30, 124.03, 102.43, 61.01, 14.16; HRMS (ESI-QTOF) m/z [M + H]$^+$ calcd for $C_{19}H_{16}NO_4$ 322.1074, found 322.1076.

*2-((3,4,5-Trimethoxyphenyl)amino)naphthalene-1,4-dione (**YQ-018**).* Red solid, mp: 1432.-144.5 °C; ^{1}H NMR (400 MHz, $CDCl_3$) δ 8.11 (dd, J = 2.4, 7.6 Hz, 2H), 7.76 (t, J = 7.4 Hz, 1H), 7.67 (t, J = 7.4 Hz, 1H), 7.46 (s, 1H), 6.49 (s, 2H), 6.34 (s, 1H), 3.87 (s, 6H), 3.86 (s, 3H); ^{13}C NMR (100 MHz, $CDCl_3$) δ 183.96, 182.15, 154.08, 145.26, 136.18, 135.12, 133.38, 133.29, 132.50, 130.46, 126.66, 126.34, 103.54, 100.85, 61.19, 56.45; HRMS (ESI-QTOF) m/z [M + H]$^+$ calcd for $C_{19}H_{18}NO_5$ 340.1179, found 340.1180.

*2-((4-Methoxyphenyl)amino)naphthalene-1,4-dione (**YQ-019**).* Brown solid, mp: 145.4−147.2 °C; ^{1}H NMR (400 MHz, $CDCl_3$) δ 8.12−8.09 (m, 2H), 7.75 (t, J = 7.6 Hz, 1H), 7.65 (t, J = 7.6 Hz, 1H), 7.44 (s, 1H), 7.20 (d, J = 8.8 Hz, 2H), 6.95 (d, J = 5.2 Hz, 2H), 6.22 (s, 1H), 3.83 (s, 3H); ^{13}C NMR (100 MHz, $CDCl_3$) δ 183.89, 182.32, 157.80, 145.81, 135.03, 133.53, 132.35, 130.55, 130.14, 126.58, 126.29, 124.99, 115.05, 102.66, 55.71; HRMS (ESI-QTOF) m/z [M + H]$^+$ calcd for $C_{17}H_{14}NO_3$ 280.0968, found 280.0967.

*7-(Phenylamino)isoquinoline-5,8-dione (**YQ-020**).* Orange solid, mp: 190.2−193 °C; ^{1}H NMR (400 MHz, $CDCl_3$) δ 9.34 (s, 1H), 9.05 (d, J = 4.8 Hz, 1H), 7.91 (d, J = 4.8 Hz, 1H), 7.70−7.52 (m, 2H), 7.44 (t, J = 7.6 Hz, 2H), 7.28 (d, J = 7.6 Hz, 2H), 6.47 (s, 1H); ^{13}C NMR (100 MHz, $CDCl_3$) δ 182.18, 181.61, 156.59, 148.25, 145.03, 138.79, 136.87, 129.97, 126.47, 124.23, 123.16, 118.90, 103.72; HRMS (ESI-QTOF) m/z [M + H]$^+$ calcd for $C_{15}H_{11}N_2O_2$ 251.0815, found 251.0816.

*7-((4-Fluorophenyl)amino)isoquinoline-5,8-dione (**YQ-021**).* Brown solid, mp: 261.2−263.8 °C; ^{1}H NMR (400 MHz, DMSO-d_6) δ 9.49 (s, 1H), 9.20 (s, 1H), 9.06 (d, J = 4.8 Hz, 1H), 7.81 (d, J = 4.8 Hz, 1H), 7.44−7.39 (m, 2H), 7.33−7.28 (m, 2H), 6.05 (s, 1H); ^{13}C NMR (100 MHz, DMSO-d_6) δ 181.11, 158.44, 156.10, 147.25, 146.96, 138.15, 133.97, 126.37, 124.51, 118.13, 116.32, 116.09, 102.00; HRMS (ESI-QTOF) m/z [M + H]$^+$ calcd for $C_{15}H_{10}FN_2O_2$ 269.0721, found 269.0726.

*7-((4-Iodophenyl)amino)isoquinoline-5,8-dione (**YQ-022**).* Purple solid, mp: 239.2−240.1 °C; ^{1}H NMR (400 MHz, $CDCl_3$) δ 9.35 (s, 1H), 9.06 (d, J = 5.2 Hz, 1H), 7.92 (d, J = 4.8 Hz, 1H), 7.76 (d, J =

DOI: 10.1021/acschemneuro.9b00093
ACS Chem. Neurosci. XXXX, XXX, XXX−XXX

8.4 Hz, 2H), 7.56 (s, 1H), 7.05 (d, J = 8.4 Hz, 3H), 6.45 (s, 1H); ^{13}C NMR (100 MHz, $CDCl_3$) δ 182.21, 181.41, 156.73, 148.35, 144.47, 139.05, 138.63, 136.76, 124.67, 124.12, 118.93, 104.29, 90.28; HRMS (ESI-QTOF) m/z $[M + H]^+$ calcd for $C_{15}H_{10}IN_2O_2$ 376.9781, found 376.9782.

7-(p-Tolylamino)isoquinoline-5,8-dione (**YQ-023**). Black solid, mp: 218.4−223.6 °C; ^{1}H NMR (400 MHz, $CDCl_3$) δ 9.33 (s, 1H), 9.04 (d, J = 4.8 Hz, 1H), 7.91 (d, J = 4.8 Hz, 1H), 7.58 (s, 1H), 7.24 (d, J = 8.4 Hz, 2H), 7.17 (d, J = 8.0 Hz, 2H), 6.41 (s, 1H), 2.38 (s, 3H); ^{13}C NMR (100 MHz, $CDCl_3$) δ 182.08, 181.70, 156.58, 148.23, 145.28, 138.93, 136.58, 134.17, 130.53, 124.28, 123.21, 118.92, 103.42, 21.19; HRMS (ESI-QTOF) m/z $[M + H]^+$ calcd for $C_{16}H_{13}N_2O_2$ 265.0972, found 265.0971.

2-(Phenylamino)naphthalene-1,4-dione (**YQ-024**). Red solid, mp: 192.7−193.3 °C; ^{1}H NMR (400 MHz, $CDCl_3$) δ 8.12 (t, J = 7.4 Hz, 2H), 7.77 (t, J = 7.6 Hz, 1H), 7.67 (t, J = 7.4 Hz, 1H), 7.57 (s, 1H), 7.42 (t, J = 7.8 Hz, 2H), 7.28 (d, J = 7.6 Hz, 2H), 7.22 (t, J = 7.4 Hz, 1H), 6.42 (s, 1H); ^{13}C NMR (100 MHz, $CDCl_3$) δ 184.10, 182.23, 144.88, 137.57, 135.08, 133.37, 132.51, 130.51, 129.85, 126.69, 126.32, 125.79, 122.77, 103.54; HRMS (ESI-QTOF) m/z $[M + H]^+$ calcd for $C_{16}H_{12}NO_2$ 250.0863, found 250.0864.

6-Chloro-7-(phenylamino)isoquinoline-5,8-dione (**YQ-025**). Purple solid, mp: 252.4−254.2 °C; ^{1}H NMR (400 MHz, $CDCl_3$) δ 9.35 (s, 1H), 9.07 (d, J = 4.8 Hz, 1H), 8.00 (d, J = 5.2 Hz, 1H), 7.80 (s, 1H), 7.38 (t, J = 7.6 Hz, 2H), 7.28 (d, J = 7.6 Hz, 1H), 7.11 (d, J = 8 Hz, 2H); ^{13}C NMR (100 MHz, $CDCl_3$) δ 180.08, 176.24, 156.77, 155.01, 148.70, 141.66, 138.22, 136.93, 128.70, 126.53, 124.86, 124.58, 119.55; HRMS (ESI-QTOF) m/z $[M + H]^+$ calcd for $C_{15}H_{10}ClN_2O_2$ 285.0425, found 285.0423.

6-Chloro-7-((4-iodophenyl)amino)isoquinoline-5,8-dione (**YQ-026**). Brown solid, mp: 267.6−271.1 °C; ^{1}H NMR (400 MHz, DMSO-d_6) δ 9.56 (s, 1H), 9.17 (s, 1H), 9.07 (d, J = 4.8 Hz, 1H) 7.89 (d, J = 5.2 Hz, 1H), 7.66 (d, J = 8.4 Hz, 2H), 6.97 (d, J = 8.4 Hz, 2H); ^{13}C NMR (100 MHz, DMSO-d_6) δ 179.63, 175.83, 155.90, 147.54, 143.28, 138.62, 137.56, 136.63, 126.12, 125.77, 124.35, 118.61, 89.07; HRMS (ESI-QTOF) m/z $[M + H]^+$ calcd for $C_{15}H_9ClIN_2O_2$ 410.9392, found 410.9391.

6-Chloro-7-(p-tolylamino)isoquinoline-5,8-dione (**YQ-027**). Purple solid, mp: 263.3−265.6 °C; ^{1}H NMR (400 MHz, $CDCl_3$) δ 9.34 (s, 1H), 9.06 (d, J = 4.8 Hz, 1H), 7.99 (d, J = 4.8 Hz, 1H), 7.77 (s, 1H), 7.17 (d, J = 7.6 Hz, 2H), 7.01 (d, J = 7.6 Hz, 2H), 2.38 (s, 3H); ^{13}C NMR (100 MHz, $CDCl_3$) δ 180.13, 156.74, 154.91, 149.09, 148.67, 141.79, 138.31, 136.62, 134.34, 129.28, 124.89, 124.65, 119.54, 21.24; HRMS (ESI-QTOF) m/z $[M + H]^+$ calcd for $C_{16}H_{12}ClN_2O_2$ 299.0582, found 299.0583.

7-((4-Bromophenyl)amino)-6-chloroisoquinoline-5,8-dione (**YQ-028**). Purple solid, mp: 293.8−294.7 °C; ^{1}H NMR (400 MHz, DMSO-d_6) δ 9.57 (s, 1H), 9.17 (s, 1H), 9.07 (d, J = 4.8 Hz, 1H), 7.89 (d, J = 5.2 Hz, 1H). 7.51 (d, J = 8.8 Hz, 2H), 7.11 (d, J = 8.4 Hz, 2H); ^{13}C NMR (100 MHz, DMSO-d_6) δ 179.62, 175.85, 155.91, 147.54, 143.40, 138.17, 137.56, 130.80, 125.96, 124.36, 118.62, 116.84, 115.08; HRMS (ESI-QTOF) m/z $[M + H]^+$ calcd for $C_{15}H_9BrClN_2O_2$ 362.9530, found 362.9533.

6-Chloro-7-((4-methoxyphenyl)amino)isoquinoline-5,8-dione (**YQ-029**). Black solid, mp: 225.6−227.6 °C; ^{1}H NMR (400 MHz, $CDCl_3$) δ 9.33 (s, 1H), 9.05 (d, J = 5.2 Hz, 1H), 7.99 (d, J = 4.8 Hz, 1H), 7.75 (s, 1H), 7.07 (d, J = 8.8 Hz, 2H), 6.89 (d, J = 8.8 Hz, 2H), 3.84 (s, 3H); ^{13}C NMR (100 MHz, $CDCl_3$) δ 180.12, 176.10, 158.41, 156.74, 148.64, 141.97, 138.37, 129.78, 126.73, 126.56, 123.59, 119.54, 113.87, 55.66; HRMS (ESI-QTOF) m/z $[M + H]^+$ calcd for $C_{16}H_{12}ClN_2O_3$ 315.0531, found 315.0531.

6-Chloro-7-((2-iodophenyl)amino)isoquinoline-5,8-dione (**YQ-030**). Purple solid, mp: 216.8−218.6 °C; ^{1}H NMR (400 MHz, DMSO-d_6) δ 9.55 (s, 1H), 9.17 (s, 1H), 9.06 (d, J = 4.8 Hz, 1H), 7.89 (d, J = 4.4 Hz, 1H), 7.33 (t, J = 7.6 Hz, 2H), 7.16 (d, J = 8.0 Hz, 2H); ^{13}C NMR (100 MHz, DMSO-d_6) δ 179.72, 175.70, 155.94, 147.55, 143.55, 138.59, 137.68, 136.65, 128.00, 126.15, 124.92, 124.37, 124.02, 118.65, 114.03; HRMS (ESI-QTOF) m/z $[M + H]^+$ calcd for $C_{15}H_9ClIN_2O_2$ 410.9392, found 410.9392.

6-Chloro-7-((3,4,5-trimethoxyphenyl)amino)isoquinoline-5,8-dione (**YQ-031**). Purple solid, mp: 166.2−169.8 °C; ^{1}H NMR (400 MHz, $CDCl_3$) δ 9.33 (s, 1H), 9.06 (d, J = 4.8 Hz, 1H), 7.99 (d, J = 4.8 Hz, 1H), 7.78 (s, 1H), 6.34 (s, 2H), 3.86 (s, 3H), 3.84 (s, 6H); ^{13}C NMR (100 MHz, $CDCl_3$) δ 180.03, 176.24, 156.79, 153.07, 148.68, 141.58, 138.25, 136.75, 132.55, 123.52, 119.54, 114.51, 102.94, 61.23, 56.38; HRMS (ESI-QTOF) m/z $[M + H]^+$ calcd for $C_{18}H_{16}ClN_2O_5$ 375.0742, found 375.0742.

7-((4-Chlorophenyl)amino)isoquinoline-5,8-dione (**YQ-032**). Purple solid, mp: 258−261.2 °C; ^{1}H NMR (400 MHz, $CDCl_3$) δ 9.35 (s, 1H), 9.06 (d, J = 5.2 Hz, 1H), 7.91 (d, J = 4.4 Hz, 1H), 7.57 (s, 1H), 7.42 (d, J = 8.4 Hz, 2H), 7.23 (d, J = 8.8 Hz, 2H), 6.41 (s, 1H); ^{13}C NMR (100 MHz, $CDCl_3$) δ 182.19, 181.42, 156.71, 148.33, 144.79, 138.67, 135.48, 131.89, 130.17, 124.39, 124.14, 118.94, 104.06; HRMS (ESI-QTOF) m/z $[M + H]^+$ calcd for $C_{15}H_{10}ClN_2O_2$ 285.0425, found 285.0426.

4-((5,8-Dioxo-5,8-dihydroisoquinolin-7-yl)amino)benzonitrile (**YQ-033**). Brown solid, mp: 392 °C (decomposed); ^{1}H NMR (400 MHz, $CDCl_3$) δ 9.38 (s, 1H), 9.10 (d, J = 5.2 Hz, 1H), 7.93 (d, J = 4.8 Hz, 1H), 7.74 (d, J = 8.4 Hz, 3H), 7.39 (d, J = 8.4 Hz, 2H), 6.63 (s, 1H); ^{13}C NMR (100 MHz, $CDCl_3$) δ 156.73, 148.37, 113.91, 121.84, 118.75, 105.80; HRMS (ESI-QTOF) m/z $[M + H]^+$ calcd for $C_{16}H_{10}N_3O_2$ 276.0768, found 276.0767.

Ethyl 3-((5,8-dioxo-5,8-dihydroisoquinolin-7-yl)amino)benzoate (**YQ-034**). Red solid, mp: 157.9−161 °C; ^{1}H NMR (400 MHz, $CDCl_3$) δ 9.35 (s, 1H), 9.06 (d, J = 4.4 Hz, 1H), 7.94−7.91 (m, 3H), 7.69 (s, 1H), 7.55−7.47 (m, 2H), 6.45 (s, 1H), 4.40 (q, J = 7.2 Hz, 2H), 1.41 (t, J = 7.0 Hz, 3H); ^{13}C NMR (100 MHz, $CDCl_3$) δ 182.24, 181.40, 165.62, 156.67, 148.32, 144.86, 138.65, 137.21, 132.52, 130.04, 127.39, 127.18, 124.18, 118.91, 118.12, 104.11, 61.65, 14.45; HRMS (ESI-QTOF) m/z $[M + H]^+$ calcd for $C_{18}H_{15}N_2O_4$ 323.1026, found 323.1024.

2-((4-Iodophenyl)amino)naphthalene-1,4-dione (**YQ-035**). Purple solid, mp: 234.4−237.1 °C; ^{1}H NMR (400 MHz, $CDCl_3$) δ 8.12 (t, J = 6.6 Hz, 2H), 7.79−7.66 (m, 4H), 7.51 (s, 1H), 7.04 (d, J = 8.4 Hz, 2H), 6.40 (s, H); ^{13}C NMR (100 MHz, $CDCl_3$) δ 184.02, 181.99, 144.29, 138.87, 137.47, 135.18, 133.22, 132.67, 130.41, 126.76, 126.39, 124.27, 104.18, 89.27; HRMS (ESI-QTOF) m/z $[M + H]^+$ calcd for $C_{16}H_{11}INO_2$ 375.9829, found 375.9829.

1H-Pyrrolo[3,2-g]isoquinoline-4,9-dione (**YQ-036**). Yellow solid, mp: 295.6−296.3 °C; ^{1}H NMR (400 MHz, DMSO-d_6) δ 13.14 (s, 1H), 9.20 (s, 1H), 9.04 (d, J = 4.4 Hz, 1H), 7.90 (d, J = 4.8 Hz, 1H), 7.44 (s, 2H), 6.76 (s, 1H); ^{13}C NMR (100 MHz, DMSO-d_6) δ 179.87, 174.77, 155.74, 147.71, 139.73, 132.50, 128.93, 127.43, 119.27, 108.81; HRMS (ESI-QTOF) m/z $[M + H]^+$ calcd for $C_{11}H_7N_2O_2$ 199.0502, found 199.0501.

1-Methyl-1H-pyrrolo[3,2-g]isoquinoline-4,9-dione (**YQ-037**). Yellow solid, mp: 193.7−195.4 °C; ^{1}H NMR (400 MHz, DMSO-d_6) δ 9.22 (s, 1H), 9.04 (d, J = 4.8 Hz, 1H), 7.90 (d, J = 4.8 Hz, 1H), 7.49 (d, J = 2.8 Hz, 1H), 6.74 (d, J = 2.8 Hz, 1H), 4.05 (s, 3H); ^{13}C NMR (100 MHz, DMSO-d_6) δ 176.57, 175.25, 155.60, 147.90, 139.29, 134.16, 128.14, 118.99, 107.86, 36.96; HRMS (ESI-QTOF) m/z $[M + H]^+$ calcd for $C_{12}H_9N_2O_2$ 213.0659, found 213.0660.

6-Aminoquinazoline-5,8-dione (**YQ-038**). Brown solid, mp: 304 °C (decomposed); ^{1}H NMR (400 MHz, DMSO-d_6) δ 9.52 (s, 1H), 9.25 (s, 1H), 5.97 (s, 1H); ^{13}C NMR (100 MHz, DMSO-d_6) δ 181.20, 179.42, 162.90, 155.55, 154.81, 150.74, 124.41, 104.61; HRMS (ESI-QTOF) m/z $[M + H]^+$ calcd for $C_8H_6N_3O_2$ 176.0455, found 176.0456.

7-Methyl-5H-pyrrolo[2,3-g]quinazoline-5,9(6H)-dione (**YQ-039**). Yellow solid, mp: 284 °C (decomposed); ^{1}H NMR (400 MHz, DMSO-d_6) δ 9.57 (s, 1H), 9.38 (s, 1H), 6.54 (s, 1H), 2.34 (s, 3H); ^{13}C NMR (100 MHz, DMSO-d_6) δ 178.45, 172.47, 161.97, 156.10, 155.54, 140.61, 131.10, 128.90, 126.09, 107.76, 13.12; HRMS (ESI-QTOF) m/z $[M + H]^+$ calcd for $C_{11}H_7N_3O_2$ 214.0611, found 214.0614.

Ethyl 2-(4,9-dioxo-4,9-dihydro-1H-naphtho[2,3-d][1,2,3]triazol-1-yl)acetate (**YQ-040**). Yellow solid, mp: 141.4−143.4 °C; ^{1}H NMR (400 MHz, $CDCl_3$) δ 8.33 (d, J = 7.6 Hz, 1H), 8.18 (d, J = 7.6 Hz, 1H), 7.87−7.78 (m, 2H), 5.59 (s, 2H), 4.29 (q, J = 6.8 Hz, 2H),

DOI: 10.1021/acschemneuro.9b00093
ACS Chem. Neurosci. XXXX, XXX, XXX−XXX

1.31 (t, J = 7.0 Hz, 3H); ^{13}C NMR (100 MHz, $CDCl_3$) δ 176.50, 175.42, 165.19, 145.32, 135.35, 134.30, 134.14, 133.51, 132.54, 127.94, 127.27, 62.80, 50.98, 14.06; HRMS (ESI-QTOF) m/z $[M + H]^+$ calcd for $C_{14}H_{12}N_3O_4$ 286.0822, found 286.0821.

1-(4-Methoxybenzyl)-1H-naphtho[2,3-d][1,2,3]triazole-4,9-dione (YQ-041). Brown solid, mp: 179.4−181.9 °C; ^{1}H NMR (400 MHz, $CDCl_3$) δ 8.31 (d, J = 7.2 Hz, 1H), 8.22 (d, J = 7.2 Hz, 1H), 7.81 (p, J = 7.6 Hz, 2H), 7.48 (d, J = 8.4 Hz, 2H), 6.86 (d, J = 8.0 hz, 2H), 5.95 (s, 2H), 3.77 (s, 3H); ^{13}C NMR (100 MHz, $CDCl_3$) δ 176.93, 175.51, 160.23, 145.83, 135.31, 134.41, 133.54, 132.99, 130.39, 127.98, 127.51, 126.17, 114.46, 55.44, 53.56; HRMS (ESI-QTOF) m/z $[M + H]^+$ calcd for $C_{16}H_{12}N_5O_3$ 322.0935, found 322.0939.

Animals. Male APP/PS1 double transgenic mice (B6C3-Tg-(APPswe,PSEN 1dE9)85Dbo/Mmjax) were housed in a laboratory animal breeding room in Yonsei University under regulated conditions with 12 h/12 h light−dark phase. Food and water were provided ad libitum. PCR analysis with DNA from tail biopsy following the Jackson Laboratory protocol was carried out to confirm the genotypes of APP/PS1 mice. Using the standard protocol recommended by the Jackson Laboratory, mouse brain tissues were collected at the age of 24 months for histology study. Animal care was done in accordance with the National Institutes of Health Guide for the Care and Use of Laboratory Animals and authorized by The Committee for the Care and Use of Laboratory Animals at Yonsei University.

ThT Fluorescence Assay. ThT fluorescence assay was performed to quantify the β-sheet complex of protein aggregates. Aβ42 peptides were synthesized by DMSO-incorporated Fmoc solid phase peptide synthesis protocol as previously reported.[46] For Aβ aggregation inhibition assay, in-house synthetic Aβ42 peptides and 1,4-NQ derivatives were dissolved in DMSO to prepare stocks (1 mM) and diluted with deionized water (100 μM). Aβ42 peptides were then incubated with 1,4-NQ derivatives at 37 °C for 3 days; final concentration of Aβ42 was 50 μM and that of 1,4-NQ derivatives were 0.5, 5, and 50 μM. For Aβ disaggregation assay, Aβ42 stock (100 μM) was incubated at 37 °C for 3 days to prepare Aβ aggregates. Aβ aggregates were then diluted with 1,4-NQ derivatives solutions (same concentrations as above) and reincubated for an additional 3 days at 37 °C. Twenty-five μL of the incubated samples and 75 μL of ThT (5 μM ThT in 50 mM glycine buffer, pH 8.9) were added in a 96-well half area black plate. Fluorescence intensities of ThT bound to Aβ were measured at 450 nm (excitation) and 485 nm (emission) using a microplate reader (Infinite 200 PRO, Tecan).

SDS-PAGE with PICUP. SDS-PAGE and PICUP chemistry were conducted to evaluate Aβ species by size distribution.[47,48] Because Aβ aggregates are naturally metastable, all samples were irradiated thrice (each session for 1 s) with Tris(2,2′-bipyridyl)dichlororuthenium(II) hexahydrate (1 mM) and ammonium persulfate (20 mM) to induce cross-linking before adding 5× sample buffer with β-mercaptoethanol and incubating at 90 °C for 5 min. These Aβ samples were loaded onto 1.0 mm-thick 15% gradient polyacrylamide gel (Gradi-Gel II, ELPIS) for peptide separation, and the Aβ bands were then visualized with silver staining in accordance with the PlusOne Silver Staining Kit protocol (GE Healthcare).

Fluorescent Spectral Scan. Fluorescent spectral scans were performed using a microplate reader (Infinite 200 PRO, Tecan). For excitation scans, 1,4-NQ derivatives were dissolved in DMSO to prepare 1 mM stocks before serial dilution is carried out with deionized water. Then 150 μL of the samples (50 μM) was then aliquoted to a 96-well clear round-bottom plate and the data points of the compound's excitation spectra was measured at 10 nm increments from 230 to 900 nm. The peaks for each compound were recorded as the excitation wavelengths. For emission scans, 150 μL of the same samples prepared above were transferred to a 96-well opaque round-bottom plate. The excitation wavelengths were set according to their respective compounds and the emissions were scanned at 10 nm increments at varying spectra ranges. Next, the emission spectra of the candidate compounds mixed with Aβ is needed to determine whether these compounds exhibit a fluorescence shift in the presence of Aβ. Two separate stocks of Aβ42 peptides were dissolved in DMSO (1 mM) and diluted with deionized water (100 μM). One stock was stored immediately at −80 °C to represent Aβ monomers and the other stock was incubated for 3 days to produce Aβ aggregates. 1,4-NQ derivatives were dissolved in DMSO (1 mM) followed by a serial dilution with deionized water (50 μM). Then 25 μL of Aβ monomers or aggregates and 75 μL of 1,4-NQ derivatives were added to each well in a 96-well opaque round-bottom plate. The emission spectra of the compounds with Aβ were recorded following the same process as the emission scan.

Histochemistry of APP/PS1 Double Transgenic Mouse Brains. Brain tissues were fixed in 4% paraformaldehyde overnight at 4 °C and immersed in 30% sucrose for 48 h to induce cryoprotection. Sections of 35 μm were cut with a cryostat (CM1860, Leica). For brain staining, antigen retrieval on aldehyde-fixed brain sections was performed with 1% SDS in PBS. Sections were blocked with 20% horse serum in PBS for 1 h before overnight incubation at 4 °C with mouse monoclonal antibody 6E10 (1:200), the primary antibody that detects Aβ plaques. Following an overnight incubation, a secondary goat anti-mouse IgG conjugated with Alexa fluor 555 (1:200) was added for 1 h. 1,4-NQ derivatives stocks in DMSO (10 mM) were diluted 500 μM in PBS and added to the sections overnight. The images of amyloid plaques in the cortex and the hippocampus were captured on a fluorescence microscope (DM500, Leica) equipped with filter cubes containing excitation and emission filters: A4 filter cube for Hoechst staining detection (data not shown, excitation filter: BP 360/40; dichromatic mirror: 400; emission filter: BP 470/40), N2.1 filter cube for 6E10 staining detection (excitation filter: BP 515−560; dichromatic mirror: 580; emission filter: LP 590), and L5 filter cube for YQ compound detection (excitation filter: BP 480/40; dichromatic mirror: 505; emission filter: BP 527/30).

Generation of Molecular Docking Models. Three-dimensional conformers for each compound were generated using BEST algorithm in Discovery Studio 2018 software (Dassault Systèmes). The conformers were energy minimized by CHARMM force field and clustered with RMSD 0.5 Å, which resulted in 36, 8, 2, and 1 distinct conformers for **YQ-002**, **YQ-003**, **YQ-030**, and **YQ-036**, respectively. All the conformers were separately used to run the global docking search by PatchDock program.[21]

The top 100 output docking structures for each compound were used to define a docking starting position in the subsequent docking simulation by Autodock vina by calculating ligand center of mass coordinates.[22] The input chemical structures were prepared by minimizing CHARMM force field in Discover Studio (full minimization function). After the docking simulations by Autodock vina for 100 different starting positions, the docking conformation with the lowest binding energy was finally selected as the most plausible docking model for each compound. The structure of Aβ (PDB ID: 2LMO) was prepared as described in our previous work.[49] All figures were created with PyMOL software (The PyMOL Molecular Graphics System, version 1.2r3pre, Schrödinger, LLC).

PAMPA Assay. PAMPA-BBB studies were performed using the PAMPA Explorer kit (pION Inc.) according to the manufacturer's instructions. Stock solutions of four 1,4-NQ derivatives were prepared in DMSO (10 mM). Each stock solution was diluted with Prisma HT buffer (pH 7.4) to a final concentration of 50 μM. Then, 200 μL of the resulting stock solution was added to each well of donor plates (n = 3). The PVDF (0.45 μm) filter membrane on the acceptor plate was coated with 5 μL of the BBB-1 lipid. Each well of the acceptor plate was filled with 200 μL of brain sink buffer. The acceptor plate was placed on the donor plate to form a sandwich; the sandwich was incubated at 37 °C for 4 h without stirring. The UV−vis spectra of the solutions for reference, acceptor, and donor plates were measured using plate reader (Infinite 200 PRO, Tecan). Effective permeability (P_e) for each compound was calculated using the PAMPA Explorer software v.3.5 (pION). Theophylline is used as a negative control, and lidocaine and progesterone are used as positive controls for this assay. Designations of CNS± were assigned by comparison with compounds that were identified in previous reports.[23]

DOI: 10.1021/acschemneuro.9b00093
ACS Chem. Neurosci. XXXX, XXX, XXX−XXX

Surface Plasmon Resonance Analysis. The surface plasmon resonance analysis was performed using a Biacore T200 instrument and CM5 sensor chips (GE Healthcare). Aβ42 stock was prepared in DMSO (10 mM) and diluted with PBS (pH 7.4) to make 1 mg/mL. The diluted Aβ42 was incubated for 1 day at 37 °C to make aggregates. PBS (pH 7.4) was used as a running buffer at 25 °C. Incubated Aβ42 aggregates were diluted 25-fold with 10 mM sodium acetate solution (pH 4.0) and fixed onto the sensor chip surface using amine coupling chemistry. The remaining activated surface groups were blocked with 1 M ethanolamine (pH 8.5) to prevent covalent binding of the analyte to the surface; the immobilization value was 1576.5 RU and the theoretical Rmax was 108 RU. Typically, one binding cycle comprised an association phase, followed by a dissociation phase, while the responses for different concentrations of the analyte were collected for multiple cycles. Removing the analyte from the ligand must be ensured after each cycle, but in this study, the high binding affinity of the analyte to the ligand made it difficult to maintain a proper surface regeneration condition. As such, single-cycle kinetics was applied by increasing the concentrations of analyte onto the ligand surface in one cycle.[50,51] **YQ-002** stock was 10 mM in DMSO and diluted with PBS-P (pH 7.4) containing 5% DMSO as a series of samples: 100, 200, 300, 400, and 500 μM. The analyte contact and dissociation time were 120 and 600 s, respectively, and the flow rate was 20 μL/min.

Statistical Analysis. All graphs were obtained with GraphPad Prism 7.0 software, and all statistical analyses were conducted with one-way ANOVA followed by Bonferroni's posthoc comparisons (*P < 0.033, **P < 0.002, ***P < 0.001). The error bars represent the standard deviation (SD).

■ ASSOCIATED CONTENT

Supporting Information

The Supporting Information is available free of charge on the ACS Publications website at DOI: 10.1021/acschemneuro.9b00093.

Full images of SDS-PAGE analysis with PICUP chemistry; excitation and emission spectral scan of selected 1,4-NQ derivatives; surface plasmon resonance analysis to confirm Aβ binding property; structural spectra of YQ compounds (PDF)

■ AUTHOR INFORMATION

Corresponding Authors

*E-mail: ikyonkim@yonsei.ac.kr (I.K.), for medicinal chemistry.

*E-mail: y.kim@yonsei.ac.kr (Y.K.), for amyloid investigation.

ORCID

Ikyon Kim: 0000-0002-0849-5517

YoungSoo Kim: 0000-0001-5029-7082

Author Contributions

N.N.S., H.J., and Y.J. contributed equally. N.N.S., H.J., Y.J., I.K., and Y.K. designed the experiments. N.N.S. and H.J. performed the in vitro and ex vivo experiments. Y.J., G.H.B., and I.K. designed and synthesized the YQ compounds. H.C.Y. and J.M.H. performed PAMPA assay. S.L. and S.B. prepared synthetic Aβ42. K.P. and S.H.Y. performed molecular docking model experiments. N.N.S., H.J., I.K., and Y.K. wrote the manuscript. All images were created by the authors for this manuscript.

Funding

This work was supported by Korea Health Industry Development Institute (KHIDI, HI18C0836010018), National Research Foundation (Basic Science Research Program NRF-2018R1A6A1A03023718, Original Technology Research Program for Brain Science NRF-2018M3C7A1021858, and NRF-2017R1A2A2A05069364), and Yonsei University (2018-22-0022).

Notes

The authors declare no competing financial interest.

■ ABBREVIATIONS

AD, Alzheimer's disease; Aβ, amyloid-β; NQ, naphthoquinones; 1,4-NQ, 1,4-naphthoquinones; ThT, Thioflavin T; B6C3Tg, APPswe, PSEN1dE9; 85Dbo/J, APP/PS1; BBB, blood-brain barrier; PAMPA, parallel artificial membrane permeability assay; PICUP, photoinduced cross-linking of unmodified proteins

■ REFERENCES

(1) Haass, C., and Selkoe, D. J. (2007) Soluble protein oligomers in neurodegeneration: lessons from the Alzheimer's amyloid beta-peptide. *Nat. Rev. Mol. Cell Biol. 8* (2), 101−12.

(2) Sevigny, J., Chiao, P., Bussiere, T., Weinreb, P. H., Williams, L., Maier, M., Dunstan, R., Salloway, S., Chen, T., Ling, Y., O'Gorman, J., Qian, F., Arastu, M., Li, M., Chollate, S., Brennan, M. S., Quintero-Monzon, O., Scannevin, R. H., Arnold, H. M., Engber, T., Rhodes, K., Ferrero, J., Hang, Y., Mikulskis, A., Grimm, J., Hock, C., Nitsch, R. M., and Sandrock, A. (2016) The antibody aducanumab reduces Aβ plaques in Alzheimer's disease. *Nature 537* (7618), 50−6.

(3) Abner, E. L., Neltner, J. H., Jicha, G. A., Patel, E., Anderson, S. L., Wilcock, D. M., Van Eldik, L. J., and Nelson, P. T. (2018) Diffuse amyloid-beta plaques, neurofibrillary tangles, and the impact of APOE in elderly persons' brains lacking neuritic amyloid plaques. *J. Alzheimer's Dis. 64* (4), 1307−1324.

(4) Babula, P., Adam, V., Havel, L., and Kizek, R. (2009) Noteworthy secondary metabolites naphthoquinones - their occurrence, pharmacological properties and analysis. *Curr. Pharm. Anal. 5*, 47−68.

(5) Widhalm, J. R., and Rhodes, D. (2016) Biosynthesis and molecular actions of specialized 1,4-naphthoquinone natural products produced by horticultural plants. *Hortic. Res. 3*, 16046.

(6) Edreva, A., Velikova, V., Tsonev, T., Dagnon, S., Gürel, A. L., and Aktaş, L. (2007) Stress-protective role of secondary metabolites: Diversity of functions and mechanisms. *Gen. Appl. Plant Physiol.*, 34.

(7) Kim, B. H., Yoo, J., Park, S. H., Jung, J. K., Cho, H., and Chung, Y. (2006) Synthesis and evaluation of antitumor activity of novel 1,4-naphthoquinone derivatives (IV). *Arch. Pharmacal Res. 29* (2), 123−30.

(8) López, L. I., Nery Flores, S. D., Silva Belmares, S. Y., and Sáenz Galindo, A. (2014) Naphthoquinones: biological properties and synthesis of lawsone and derivatives - a structured review. *Vitae 21*, 248−258.

(9) Tandon, V. K., Chhor, R. B., Singh, R. V., Rai, S., and Yadav, D. B. (2004) Design, synthesis and evaluation of novel 1,4-naphthoquinone derivatives as antifungal and anticancer agents. *Bioorg. Med. Chem. Lett. 14* (5), 1079−83.

(10) Vukic, M. D., Vukovic, N. L., Djelic, G. T., Popovic, S. L., Zaric, M. M., Baskic, D. D., Krstic, G. B., Tesevic, V. V., and Kacaniova, M. M. (2017) Antibacterial and cytotoxic activities of naphthoquinone pigments from Onosma visianii Clem. *Exp. Clin. Sci. J. 16*, 73−88.

(11) Bermejo-Bescos, P., Martin-Aragon, S., Jimenez-Aliaga, K. L., Ortega, A., Molina, M. T., Buxaderas, E., Orellana, G., and Csaky, A. G. (2010) In vitro antiamyloidogenic properties of 1,4-naphthoquinones. *Biochem. Biophys. Res. Commun. 400* (1), 169−74.

(12) Castagnoli, K. P., Steyn, S. J., Petzer, J. P., Van der Schyf, C. J., and Castagnoli, N., Jr. (2001) Neuroprotection in the MPTP Parkinsonian C57BL/6 mouse model by a compound isolated from tobacco. *Chem. Res. Toxicol. 14* (5), 523−7.

(13) Nam, K. N., Son, M. S., Park, J. H., and Lee, E. H. (2008) Shikonins attenuate microglial inflammatory responses by inhibition

DOI: 10.1021/acschemneuro.9b00093
ACS Chem. Neurosci. XXXX, XXX, XXX−XXX

of ERK, Akt, and NF-kappaB: neuroprotective implications. *Neuropharmacology 55* (5), 819−25.
(14) Scherzer-Attali, R., Pellarin, R., Convertino, M., Frydman-Marom, A., Egoz-Matia, N., Peled, S., Levy-Sakin, M., Shalev, D. E., Caflisch, A., Gazit, E., and Segal, D. (2010) Complete phenotypic recovery of an Alzheimer's disease model by a quinone-tryptophan hybrid aggregation inhibitor. *PLoS One 5* (6), No. e11101.
(15) Tomiyama, T., Shoji, A., Kataoka, K., Suwa, Y., Asano, S., Kaneko, H., and Endo, N. (1996) Inhibition of amyloid beta protein aggregation and neurotoxicity by rifampicin. Its possible function as a hydroxyl radical scavenger. *J. Biol. Chem. 271* (12), 6839−44.
(16) Munishkina, L. A., and Fink, A. L. (2007) Fluorescence as a method to reveal structures and membrane-interactions of amyloidogenic proteins. *Biochim. Biophys. Acta, Biomembr. 1768* (8), 1862−1885.
(17) Hudson, S. A., Ecroyd, H., Kee, T. W., and Carver, J. A. (2009) The thioflavin T fluorescence assay for amyloid fibril detection can be biased by the presence of exogenous compounds. *FEBS J. 276* (20), 5960−72.
(18) Bitan, G. (2006) Structural study of metastable amyloidogenic protein oligomers by photo-induced cross-linking of unmodified proteins. *Methods Enzymol. 413*, 217−236.
(19) Jameson, L. P., Smith, N. W., and Dzyuba, S. V. (2012) Dye-binding assays for evaluation of the effects of small molecule inhibitors on amyloid (abeta) self-assembly. *ACS Chem. Neurosci. 3* (11), 807−19.
(20) Meyer-Luehmann, M., Spires-Jones, T. L., Prada, C., Garcia-Alloza, M., de Calignon, A., Rozkalne, A., Koenigsknecht-Talboo, J., Holtzman, D. M., Bacskai, B. J., and Hyman, B. T. (2008) Rapid appearance and local toxicity of amyloid-beta plaques in a mouse model of Alzheimer's disease. *Nature 451* (7179), 720−4.
(21) Schneidman-Duhovny, D., Inbar, Y., Nussinov, R., and Wolfson, H. J. (2005) PatchDock and SymmDock: servers for rigid and symmetric docking. *Nucleic Acids Res. 33*, W363−7.
(22) Trott, O., and Olson, A. J. (2009) AutoDock Vina: improving the speed and accuracy of docking with a new scoring function, efficient optimization, and multithreading. *J. Comput. Chem. 31* (2), 455−61.
(23) Di, L., Kerns, E. H., Fan, K., McConnell, O. J., and Carter, G. T. (2003) High throughput artificial membrane permeability assay for blood-brain barrier. *Eur. J. Med. Chem. 38* (3), 223−232.
(24) O'Hare, E., Scopes, D. I. C., Kim, E.-M., Palmer, P., Jones, M., Whyment, A. D., Spanswick, D., Amijee, H., Nerou, E., McMahon, B., Treherne, J. M., and Jeggo, R. (2013) Orally bioavailable small molecule drug protects memory in Alzheimer's disease models. *Neurobiol. Aging 34* (4), 1116−1125.
(25) Liscic, R. M. (2013) Immunological aspects and anti-amyloid strategy for Alzheimer's dementia. *Arh. Hig. Rada Toksikol. 64* (4), 603−8.
(26) Sundaram, G. S. M., Dhavale, D. D., Prior, J. L., Yan, P., Cirrito, J., Rath, N. P., Laforest, R., Cairns, N. J., Lee, J.-M., Kotzbauer, P. T., and Sharma, V. (2016) Fluselenamyl: a novel benzoselenazole derivative for PET detection of amyloid plaques (Aβ) in Alzheimer's disease. *Sci. Rep. 6*, 35636.
(27) Viola, K. L., and Klein, W. L. (2015) Amyloid beta oligomers in Alzheimer's disease pathogenesis, treatment, and diagnosis. *Acta Neuropathol. 129* (2), 183−206.
(28) Zhang, X., Bloch, S., Akers, W., and Achilefu, S. (2012) Near-infrared molecular probes for in vivo imaging. *Curr. Protoc. Cytom. 60*, 12.27.1.
(29) Fridén, M., Wennerberg, M., Antonsson, M., Sandberg-Ställ, M., Farde, L., and Schou, M. (2014) Identification of positron emission tomography (PET) tracer candidates by prediction of the target-bound fraction in the brain. *EJNMMI Res. 4* (1), 50−50.
(30) Pike, V. W. (2009) PET radiotracers: crossing the blood-brain barrier and surviving metabolism. *Trends Pharmacol. Sci. 30* (8), 431−40.
(31) Klunk, W. E., and Mathis, C. A. (2008) The future of amyloid-beta imaging: a tale of radionuclides and tracer proliferation. *Curr. Opin. Neurol. 21* (6), 683−687.
(32) Biancalana, M., and Koide, S. (2010) Molecular mechanism of Thioflavin-T binding to amyloid fibrils. *Biochim. Biophys. Acta, Proteins Proteomics 1804* (7), 1405−1412.
(33) Groenning, M. (2010) Binding mode of Thioflavin T and other molecular probes in the context of amyloid fibrils-current status. *Journal of Chemical Biology 3* (1), 1−18.
(34) Teoh, C. L., Su, D., Sahu, S., Yun, S.-W., Drummond, E., Prelli, F., Lim, S., Cho, S., Ham, S., Wisniewski, T., and Chang, Y.-T. (2015) Chemical fluorescent probe for detection of Aβ oligomers. *J. Am. Chem. Soc. 137* (42), 13503−13509.
(35) Bhasin, D., Chettiar, S. N., Etter, J. P., Mok, M., and Li, P. K. (2013) Anticancer activity and SAR studies of substituted 1,4-naphthoquinones. *Bioorg. Med. Chem. 21* (15), 4662−9.
(36) Koller, A., Rudi, A., Gravalos, M. G., and Kashman, Y. (2001) Synthesis and electrophilic substitution of pyrido[2,3,4-kl]- acridines. *Molecules 6* (4), 300−322.
(37) Anderson, W. P., Connarty, B., and El-Hajj, T. (1986) A simple efficient synthesis of 5,8-Isoquinolinedione. *Synth. Commun. 16*, 1557−1560.
(38) Kitahara, Y., Nakai, T., Nakahara, S., Akazawa, M., Shimizu, M., and Kubo, A. (1991) Synthesis of 5, 6-, 5, 8- and 7, 8-isoquinolinediones from the corresponding isoquinolinols and dimethoxyisoquinolines. *Chem. Pharm. Bull. 39* (9), 2256−2263.
(39) Ryu, C.-K., Lee, I. K., Jung, S. H., Kang, H. Y., and Lee, C. O. (2000) 7-(Substituted-phenyl)amino-5,8-isoquinolinediones: Synthesis and cytotoxic activities on cancer cell lines. *Med. Chem. Res. 10*, 40−49.
(40) Ryu, C.-K., Jeong, H.-J., Lee, S. K., You, H.-J., Choi, K. U., Shim, J.-Y., Heo, Y. H., and Lee, C.-O. (2001) Effects of 6-arylamino-5,8-quinolinediones and 6-chloro-7-ary-lamino-5,8-isoquinolinediones on NAD(P)H: quinone oxidoreductase (NQO1) activity and their cytotoxic potential. *Arch. Pharmacal Res. 24* (5), 390−396.
(41) Leepasert, T., Shahabi, M., Shanab, K., Schirmer, E., Holzer, W., Spreitzer, H., Aicher, B., Müller, G., and Günther, E. (2013) Synthesis and antiproliferative activity of new cytotoxic tri- and tetraazabenzo[3,2-a]fluorene-5,6-dione derivatives. *Bioorg. Med. Chem. Lett. 23* (19), 5264−5266.
(42) Wu, Y.-L., Chuang, C.-P., and Lin, P.-Y. (2001) Oxidative free radical reactions between 2-amino-1,4-naphthoquinones and carbonyl compounds. *Tetrahedron 57* (26), 5543−5549.
(43) Shanab, K., Schirmer, E., Knafl, H., Wulz, E., Holzer, W., Spreitzer, H., Schmidt, P., Aicher, B., Müller, G., and Günther, E. (2010) Synthesis and biological evaluation of new cytotoxic azanaphthoquinone pyrrolo-annelated derivatives. *Bioorg. Med. Chem. Lett. 20* (13), 3950−3952.
(44) Kitahara, Y., Nakahara, S., Tanaka, Y., and Kubo, A. (1992) Synthesis of 5,8-quinoxalinediones and 5,8-quinazolinediones. *Heterocycles 34*, 1623−1630.
(45) Fosso, M. Y., Chan, K. Y., Gregory, R., and Chang, C.-W. T. (2012) Library synthesis and antibacterial investigation of cationic anthraquinone analogs. *ACS Comb. Sci. 14* (3), 231−235.
(46) Lee, S., and Kim, Y. (2015) Anti-amyloidogenic approach to access amyloid-β(1−42) in Fmoc solid-phase synthesis. *Bulletin of the Korean Chemical Society 36* (8), 2147−2149.
(47) Bitan, G., and Teplow, D. B. (2004) Rapid photochemical cross-linking–a new tool for studies of metastable, amyloidogenic protein assemblies. *Acc. Chem. Res. 37* (6), 357−64.
(48) Rahimi, F., Maiti, P., and Bitan, G. (2009) Photo-induced cross-linking of unmodified proteins (PICUP) applied to amyloidogenic peptides. *J. Visualized Exp.* No. 23, e1071.
(49) Yang, S. H., Lee, D. K., Shin, J., Lee, S., Baek, S., Kim, J., Jung, H., Hah, J. M., and Kim, Y. (2017) Nec-1 alleviates cognitive impairment with reduction of Abeta and tau abnormalities in APP/PS1 mice. *EMBO Mol. Med. 9* (1), 61−77.

DOI: 10.1021/acschemneuro.9b00093
ACS Chem. Neurosci. XXXX, XXX, XXX−XXX

(50) Karlsson, R., Katsamba, P. S., Nordin, H., Pol, E., and Myszka, D. G. (2006) Analyzing a kinetic titration series using affinity biosensors. *Anal. Biochem. 349* (1), 136−147.
(51) Myszka, D. G., Jonsen, M. D., and Graves, B. J. (1998) Equilibrium analysis of high affinity interactions using BIACORE. *Anal. Biochem. 265* (2), 326−330.

DOI: 10.1021/acschemneuro.9b00093
ACS Chem. Neurosci. XXXX, XXX, XXX−XXX